

Daniel Oyeghe Blasco

Nanoporous Alumina as Drug Delivery Systems

Final Degree Project
directed by Dr. Lluís F. Marsal

Bachelor's degree in Biomedical Engineering



UNIVERSITAT ROVIRA I VIRGILI

Tarragona

2023

Acknowledgments

First and foremost, I am deeply grateful to my supervisor, Dr. Lluís Marsal, for his guidance, expertise, and unwavering support throughout this research project. His valuable insights and feedback have greatly contributed to the quality of this work.

I would like to extend a special and heartfelt thank you to Dr. Pilar Formentín. Her exceptional dedication, consistent support, and genuine interest in my progress have been instrumental to the successful completion of this thesis. From the outset, she provided invaluable guidance and took a keen interest in my research, always encouraging me to explore new avenues and pushing me to reach my full potential. Her meticulous attention to detail, prompt feedback, and insightful suggestions have significantly enhanced the quality and rigor of this study. I am truly grateful for her unwavering belief in my abilities and her continuous support throughout this journey.

I would also like to express my gratitude to the laboratory group, particularly Josep Maria Cantons, for their collaboration, knowledge-sharing, and assistance. Their contributions and expertise have been invaluable in shaping the outcomes of this research.

Lastly, I want to acknowledge the unwavering support of my family and friends. Their love, encouragement, and understanding have been my constant motivation and a source of strength.

To all those who have contributed to this thesis in various ways, I extend my deepest appreciation. Your support and guidance have been invaluable, and I am truly grateful for the opportunity to work alongside such remarkable individuals.

Summary

This final degree project investigates the use of nanoporous anodic alumina structures for controlled drug release. The study focuses on comparing inverted funnel-like structures with regular pores and explores their fabrication and design parameters. By implementing annealing, second anodization, and pore widening techniques, significant improvements in pore characteristics were achieved, allowing for greater control over drug release kinetics. The findings highlight the potential of nanoporous anodic alumina structures in tailoring drug delivery profiles and advancing pharmaceutical sciences.

Índex

1	Introduction	1
1.1	Drug Delivery Systems.....	1
1.2	Nanoporous Anodic Alumina principles	3
1.2.1	Nanostructured Anodic Alumina's history.....	3
1.2.2	Basis for the Formation of Nanoporous Anodic Alumina.....	4
1.2.3	Nanoporous Anodic Alumina Structure	5
1.2.4	Geometrical Parameters	8
2	Nanoporous Anodic Alumina Fabrication	10
2.1	Experimental Setup	10
2.1.1	Electrochemical Cell	10
2.1.2	Software	12
2.1.3	Aluminium Substrate	12
2.2	Pre-treatments.....	13
2.3	Two-step Anodization	14
2.4	Post-treatments	18
2.4.1	Annealing.....	18
2.4.2	Pore Widening.....	18
2.5	New Pore Architecture: Inverted Funnels-like Pores.....	19
3	Characterization of NAA structures	20
4	Results and Discussion	22
4.1	Fabrication of Alumina Structures	22
4.1.1	NAA Structures Using Phosphoric Acid	22
4.1.2	NAA structures Using Oxalic Acid.....	23
4.1.3	Inverted Funnels Structures.....	25
4.2	Drug Release Based of Nanoporous Anodic Alumina	30
4.2.1	Drug Loading	30
4.2.2	Drug Release.....	31
5	Conclusions.....	38
6	References.....	39

1 Introduction

1.1 Drug Delivery Systems

Modern medicine depends heavily on drug delivery methods to increase the efficacy, convenience, and safety of medicinal therapies. A wide variety of strategies are used in the field of drug delivery systems to get therapeutic medicines to the intended location of action in the body.

In the 20th century, the pharmaceutical industry experienced significant growth, and new drug delivery systems were developed to improve the efficacy and safety of drug treatments. In the 1960s, the first sustained-release drug delivery system was introduced, allowing for controlled drug release over an extended period of time. This approach reduced the need for frequent dosing and improved patient convenience and adherence to treatment regimens.

We can also follow the development of controlled drug delivery back to the 1960s, when a variety of macroscopic "controlled" drug delivery implants and devices were developed for use as mucosal inserts (in the eye), implants (sub-cutaneous or intramuscular), ingestible capsules (using the gastrointestinal tract), topical patches (on the skin), and implants. The period of microscopic degradable polymers began in the 1980s, and we are currently living in the exciting and very active nanoscopic era [1].

The 1970s saw the development of targeted drug delivery systems, which aim to deliver drugs to specific cells or tissues in the body while minimizing off-target effects. One early example of targeted drug delivery was the development of liposomal formulations, which encapsulate drugs within lipid vesicles and allow for targeted delivery to specific tissues.

In the 21st century, drug delivery systems continue to evolve and expand. Advances in nanotechnology have led to the development of new drug delivery approaches using nanoparticles, which can improve drug efficacy and bioavailability. Other innovations include the development of implantable devices for continuous drug delivery and the use of gene therapy to deliver therapeutic genes to cells in the body.

Overall, the history of drug delivery systems has been characterized by a constant drive to improve the efficacy, safety, and convenience of drug treatments. The development of new drug delivery systems continues to offer new opportunities for personalized and targeted drug therapy, with the potential to transform the landscape of modern medicine.

The development of recent scientific techniques for nanoscale material structure has piqued the scientific community's curiosity. The ability to modify matter at the nanoscale has made it possible to create and analyze materials that, as a result of their unique nanostructural characteristics, exhibit novel and unusual phenomena [2]. Biomaterials are becoming more and more necessary for a wide range of applications. They can be implanted for a few days to several decades in long-term applications or used for short-term purposes like surgical operations. Growing interest in creating drug delivery systems that are effective for treating a variety of diseases with minimal adverse effects is also seen. Understanding the processes driving the evolution of the medications in the body as they are supplied under specific conditions and via a specific administration route is necessary to be able to comprehend how drug administration functions appropriately [3].

One such limitation is systemic toxicity, which can occur when a drug is distributed throughout the body, rather than being targeted to a specific site. For example, oral pills are often absorbed into the bloodstream and can have off-target effects, leading to adverse side

effects. Similarly, injections can result in the rapid and widespread distribution of a drug, potentially causing systemic toxicity [4].

Another limitation is poor bioavailability, which refers to the amount of a drug that actually reaches its intended target in the body. Oral pills, for example, can be degraded by stomach acid or metabolized by enzymes in the liver before they reach their target, leading to lower bioavailability. Topical creams may also have limited bioavailability due to the skin barrier [5].

Finally, many traditional drug delivery methods require frequent dosing to maintain therapeutic levels of a drug in the body. This can be inconvenient for patients and can increase the risk of non-adherence to treatment regimens [6].

To address these limitations, drug delivery systems have evolved to encompass a range of innovative approaches. These include targeted drug delivery systems that direct drugs to specific cells or tissues in the body, sustained-release formulations that allow for controlled drug release over time, and implantable devices that provide continuous drug delivery.

Drug delivery systems also enable the development of personalized medicine, as they allow for the customization of drug delivery to individual patients based on their unique needs and conditions. This can improve treatment outcomes and reduce the risk of adverse side effects.

Overall, drug delivery systems play a critical role in modern medicine by improving the safety, efficacy, and convenience of drug treatments. The development of innovative drug delivery approaches, such as the use of alumina nanoparticles, continues to expand the scope of drug delivery systems and offer new opportunities for targeted and personalized drug therapy.

The medicine needs to go through five separate procedures or stages. The initials of these five stages, which typically describe the temporal and spatial evolution of a medication after being supplied to an organism under predetermined circumstances and using a certain administration method, are combined to form the acronym LADME. Liberation (drug release), Absorption, Distribution, Metabolism, and Excretion are the stages involved. Since we are doing in vitro experiments and are interested in the release variations employing nanoporous alumina with various chemical characteristics, we will concentrate the studies in this study on the first stage: liberation [7].

The goal of the new drug delivery systems is to speed up the delivery of the drug to a specific area of the body. Additionally, it is necessary to maintain the proper focus for the required period of time and location. This location may be intrasular (inside a tissue), intracellular (within a cell), or extrasular (outside a tissue), such as the intestinal lumen.

The essential goal of the systems that regulate drug release is to enhance drug administration by decreasing adverse effects and extending the therapeutic benefit while keeping plasmatic concentrations in the organism between the maximum safe and minimum effective levels. Using controlled release devices, it is possible to keep the drug concentration between the two limits for a long time with just one dose. The majority of our efforts in this endeavour will be directed on this kind of controlled release method.

Controlled drug delivery systems offer promising solutions to address limitations such as poor biodistribution, tissue injury, drug breakdown, cytotoxicity, and adverse effects [8,9]. Nanoporous anodic alumina (NAA) has emerged as a favorable substance for drug delivery due to its biocompatibility, stability, and controlled pore geometry. It has been investigated in various domains, including transplanted cell carriers, therapeutic devices for tissue engineering, and coronary stent implants. The majority of medications on the market are hydrophobic, which limits their effectiveness [10]. Advancements in nanoscale materials have

accelerated the development of drug delivery systems, particularly for treating life-threatening diseases like cancer and heart disease. Nanoporous and nanotube carriers possess unique properties, such as low-cost fabrication, tailored surface chemistry, and high loading capacity, making them integral to drug delivery technology. Sustained-release and controlled-release drug delivery methods are employed to mitigate oscillations in drug plasma levels, reduce side effects, and improve therapeutic efficacy. By extending the duration of drug activity, sustained-release dosage forms provide longer-lasting effects, while controlled-release systems deliver drugs at specific release rates within predetermined timeframes. Utilizing NAA, a controlled-release drug delivery system is proposed. NAA's highly ordered nanoporous structure can be precisely regulated by adjusting anodization parameters, allowing for tailored drug release [11,12]. With its hardness, high surface area, and excellent chemical and thermal stability, NAA has diverse applications in infection treatment, tissue regeneration, and continuous drug administration. The controlled manipulation of pore size and depth enables effective regulation of drug release from porous materials, emphasizing the importance of pore engineering in achieving desired therapeutic outcomes [13].

1.2 Nanoporous Anodic Alumina principles

The history and current situation of nanoporous anodic alumina (NAA) are discussed in this chapter. Also accurately presented are the electrochemical mechanisms, pore ordering techniques, and anodization factors that form the basis of NAA production. Despite the fact that the structural NAA features are caused by the anodizing parameters, we have revealed the anodization parameters and those parameters independently. The final table in this chapter demonstrates their close relationship.

1.2.1 Nanostructured Anodic Alumina's history

The electrochemical oxidation of aluminum first occurred in 1920. By that time, they were exploring for methods to make decorative or protective metal layers for use in industry. Aluminum objects exposed to ambient air develop a protective covering of aluminum oxide (alumina) in a natural process. The insight sparks various suggestions for altering the material properties. Chromic acid was employed in 1923 by Bengough-Stuart for the anodization process to protect the aluminum parts. They obtained a patent for the technique they utilized to apply anodic protection to prevent corrosion in aluminum alloys.

More recently, uses for porous alumina have been found that have enormous surface areas and extremely small pores. The first sulfuric acid anodization was patented in 1927 by Glower and O'Brien. Following that, in 1936, Carboni created a colouring technique that involved anodization in sulphuric acid followed by the use of an alternating current in a metal salt solution.

Applications for porous alumina with vast surface areas and minute pores have been discovered. Glower and O'Brien received the first sulfuric acid anodization patent in 1927. Then, in 1936, Carboni developed a colouring method involving anodization in sulphuric acid and alternating current application in a metal salt solution.

Anodic Oxide Aluminum was the subject of a review written by Diggle et al. in 1969 [14]. Theoretical models of the creation mechanisms of both the barrier-type oxide and the porous-type oxide were described in this study along with structural topographies relating to water content and anion incorporation in the oxide. Thompson and Wood published an article in the late 80s and early 90s that provided a comprehensive insight of the growth mechanisms of

alumina oxide layers and improved knowledge of the mechanism for anion incorporation in NAA structures.

In 1995, Masuda and Fukuda [15] published describing self-ordered porous alumina fabrication membrane based on a two-step replication technique.

1.2.2 Basis for the Formation of Nanoporous Anodic Alumina

Anodic alumina can be formed in two ways: without pores and with pores. If we were to anodize in neutral electrolytes (pH 5-7), like for example oxalate we would grow nonporous membranes. But for this project we have centered our attention around porous membranes using anodizations in acid electrolytes as oxalic or phosphoric.

According to thermodynamics, when aluminum is exposed to air or water, the presence of oxygen causes a spontaneous reaction that results in the formation of a thin layer of aluminum oxide. The huge negative has a thermodynamic advantage for this occurrence. Change in Gibb's free energy [16].

Aqueous solutions of sulphuric, oxalic, or phosphoric acid are typically used as the electrolyte in the anodization process of aluminum to create nanoporous anodic alumina. The anode (aluminum) and cathode (platinum wire) are submerged in the electrolyte to a certain extent. Deep pores begin to form in the aluminum surface as soon as the anodization voltage (U), which varies depending on the electrolyte, is applied between the anode and the cathode. Four zones can be identified on the anodization current density versus time (t) graph when U is constant:

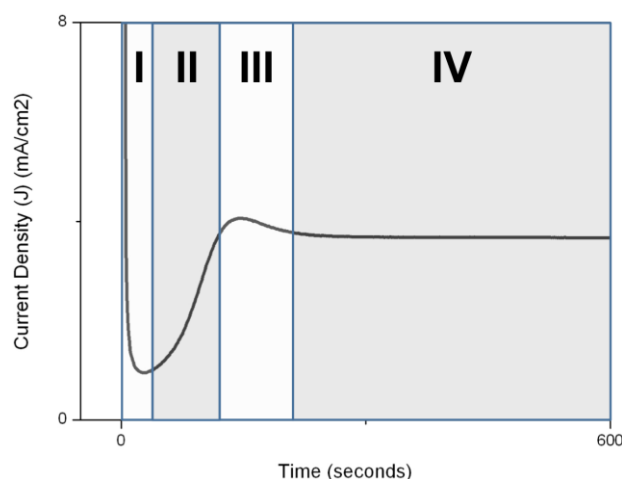


Figure 1. Current density vs. Time curve for the first 600 seconds. during the anodization of a high-purity aluminium foil under potentiostatic conditions in 0.3M oxalic acid at 40V and 5°C. Regions I, II, III and IV represent the different stages of the NAA formation.

- The presence of the electrolytic process of water in **region I** can be explained by the rapid rise in current density (J) there. The current density drops sharply as the aluminum that is in contact with the electrolyte develops a thin and compact barrier layer of aluminum oxide. In this region, the barrier layer is growing more quickly and the overall resistance is steadily increasing. When the barrier layer thickness grows, the current density (J) finally drops significantly to achieve its lowest value under the potentiostatic mode [17-19].

- The start of region II is at this place. According to a theory put forth by Parkhutik et al., actual pores can be produced through specific paths in the aforementioned oxide barrier layer. The anodization current density O is concentrated on the weak points or faults in the barrier layer that give variances in the layer settlement, according to O'Sullivan et al research on this pore formation mechanism [20]. Furthermore, Thomson et al theory states that the paths could start from the initial oxide barrier layer cracking regions due to cumulative tension stress [14, 21, 22].
- Afterwards some of the pores will cease developing, leaving behind genuine pores, while others will continue to expand. As a result of the overall diminishing resistance, the J will rise to a regional maximum value, and region III now begins. On the oxide thin layer, pores form during this region III. Pore density will decrease as a result of certain pores fusing with others. Following the achievement of a balance between the forming and dissolving aluminum oxide, area IV begins [17,19,23].

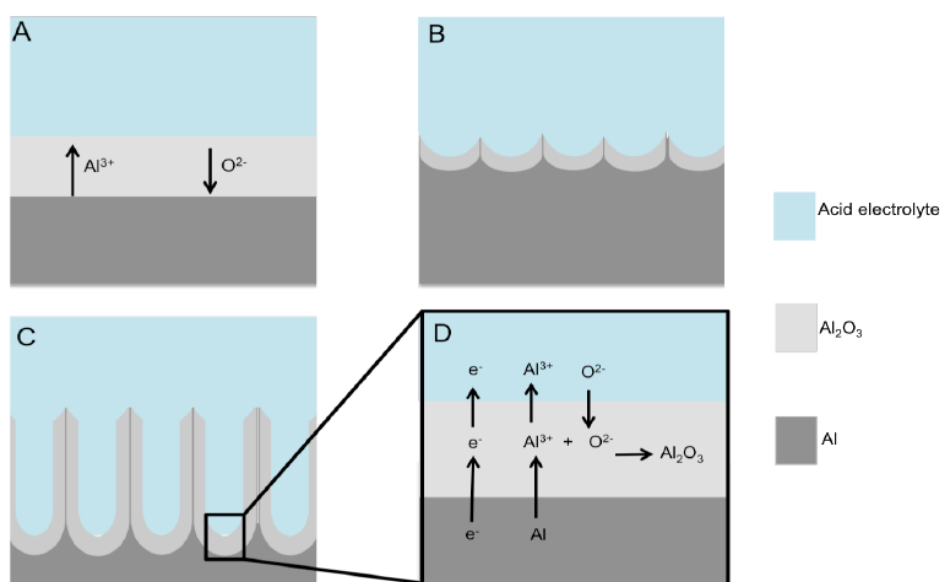


Figure 2. Schematics for the alumina pore formation. A) Formation of a thin compact layer of Al_2O_3 is formed corresponding to Region I in Figure 2.1. B) Instabilities in the electric field across the oxide film dissolve partially the oxide at certain sites; it corresponds to the Region II in Figure 2.1. C) Pore formation at the nucleation points corresponding to Region III and IV in Figure 2.1. D) Detail of the transport of the main ionic species through the oxide barrier layer.

1.2.3 Nanoporous Anodic Alumina Structure

In this project we centered our attention around the two-step anodization technique.

The self-ordering manufacture of porous NAA membranes is made possible by two-step anodization [20, 23-28]. Masuda and Fukuda first described this technique for generating self-ordered NAA using two-step anodization in 1995 [15]. They noticed that the samples' bottom pores were perfectly organized and arranged in hexagonal arrays after extensive anodization. In this manner, when the alumina is removed, a first anodization can produce an orderly pattern. Then a second anodization will provide ordered pores. It is represented in **figure 3**.

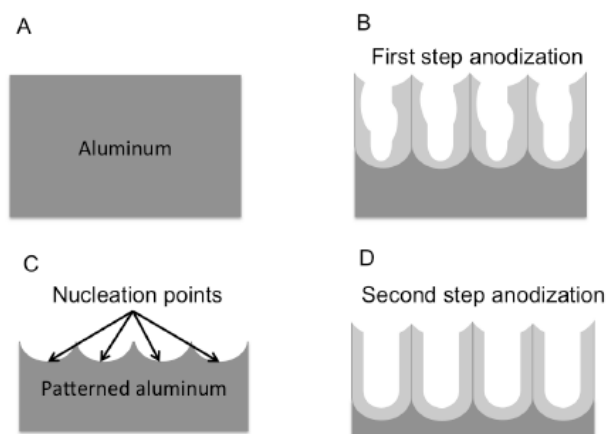


Figure 3. A) The two-step anodization starts with a flawless aluminium sheet. B) A first anodization (first step) is performed in which the pores are gaining order as they are growing deep in the aluminium bulk. C) The aluminium oxide is removed leaving a perfect ordered semi-spherical defect in the aluminium sheet. D) A second step is performed with perfectly ordered pores as a result.

The mechanical stress at the metal/oxide contact has been suggested as the cause of the self-ordering phenomenon in NAA. Al_2O_3 expands twice as much as the original volume of the aluminum substrate because its density is lower than that of the substrate made of aluminum. This volume shift induces repellent forces that result in pore organization [29].

Hexagonal unit cells make up the membranes of NAA. The skeleton, a hexagonal inner layer consisting of the shared internal walls among the unit cells, an outer layer separating the central pore from the inner layer, and an interstitial rod located inside the inner layer at the triple cell junction are the three distinct components that make up each unit cell.

As shown in figure 4, the pore structural characteristics are: pore diameter (D_p), pore wall thickness (T_w), barrier layer thickness (T_b), pore density (P), and porosity (P).

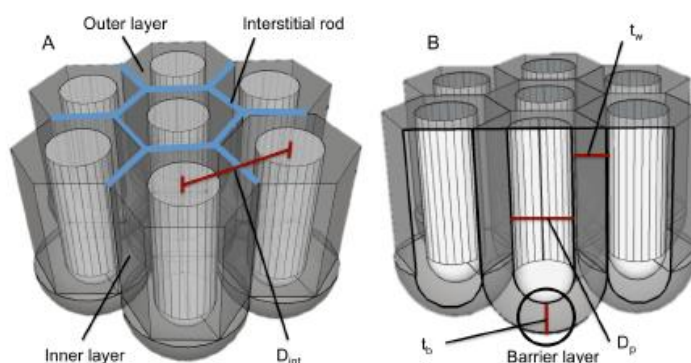


Figure 4. A) The unit cell is formed by pores equally distanced ones from others, this distance is named inter-pore distance (D_{int}). Other parts of the unit cell are: Interstitial rod, outer layer and inner layer. B) Other parameters are, the barrier layer thickness (T_b), the wall thickness (T_w) and the pore diameter (D_p).

The unit cell is made up of pores that are evenly spaced apart from one another; this separation is known as the interpore distance (D_{int}). Interstitial rod, outer layer, and inner layer are further components of the unit cell. The barrier layer thickness (T_b), wall thickness (T_w), and pore diameter (D_p) are additional factors.

As it is shown later, these characteristics are affected by the electrolyte type, anodization voltage, anodization current density, and temperature [24].

The anodization settings have control over the NAA's structural features. They are the aluminum substrate, anodization type, anodization voltage, anodization time, and electrolyte properties. Keep in mind that the pore width, interpore distance, porosity, level of hexagonal pore arrangement, and barrier layer thickness are the structural properties of the NAA. To ensure that the diffusion of the ionic species and temperature inside the pores is uniform, it must also be taken into account that the acid electrolyte must be agitated at the same pace during the whole etching action.

a) Anodization Type: Mild Anodization

Aluminum is anodized at low potentials and under potentiostatic circumstances to produce mild anodization (MA). It is distinguished by the NAA film's gradual linear development. Due to its consistent pore size (D_p) and interpore distance (D_{int}), which can be easily controlled by choosing the proper anodization conditions, this anodization type is the one that is most frequently utilized in academic research [17].

b) Anodization Voltage

With a specific acid electrolyte and concentration, the anodization voltage (U) is constrained. The oxide barrier layer will break down (sometimes referred to as "burning") and the pore growth won't be uniform if the anodization voltage is too high. The conductivity rise in the barrier layer at the bottom of the pore is the cause of this phenomena. As a result, there will be a localized heating, ionization of the atoms, which produces additional electrons as a result of the energy from the electric field, and breakdown of the oxide barrier layer as a result of the preexisting fractures.

Table 1. Voltage values for every electrolyte typology while performing mild anodization.

	Oxalic Acid ($H_2C_2O_4$)	Phosphoric Acid (H_3PO_4)
Mild Anodization	40 V	195 V

c) Anodization Time

The anodization time typically regulates the NAA layer thickness. Layer thickness and time have a linear relationship under galvanostatic circumstances. However, the template thickness does not increase linearly in potentiostatic conditions. Therefore, since the relationship between layer thickness and total current charge is linear under potentiostatic conditions, it is more accurate to control the layer thickness using the total current charge when fabricating NAA with controlled thickness under such anodization conditions [30].

d) Acid Electrolyte

The composition of the electrolyte is essential for producing high-quality NAA films. Oxalic acid and phosphoric acid are typically used as acid electrolytes in the fabrication of NAA, as we have already discussed. The acid electrolyte's kind, concentration, temperature and pH, have a significant impact on the NAA's structural properties.

The rate at which pores grow is influenced by the electrolyte's temperature. A decrease in pore growth will result from a drop in electrolyte temperature. The acid electrolyte must be kept colder than room temperature to prevent the nanoporous anodic alumina from dissolving and oxide breakdown (also known as sample burning) throughout the anodizing process. Oxalic acids were handled at a temperature of 5°C. Temperatures between -6°C and a certain amount of ethanol were utilized for phosphoric acid. The preventative measure to prevent freezing.

The pore diameter is essentially affected by the pH level. The kind and concentration of the acid electrolyte determine the pH value. Low anodization voltages are required for low pH levels. This implies a decreased Al₂O₃ field-assisted dissolution and a smaller pore diameter. This explains why the pores are larger when H₃PO₄ is used as the electrolyte and smaller when H₂C₂O is utilized.

1.2.4 Geometrical Parameters

High-quality NAA films can only be produced using aluminium foils with a purity level of 99.9% or above. Otherwise, contamination or impurities in the aluminium substrate cause volume expansion and electrical field disturbances that result in structural flaws.

a) Pore Diameter

Pore diameter (D_p) has a direct proportional relationship with voltage, temperature, time, and electrolyte pH and can range from 10 to 400 nm. This implies that the pore diameter will increase with increasing values of these parameters. The following equation can be used to calculate the pore diameter (D_p):

$$D_{int} = D_p + 2t_w$$

Equation 1. D_{int} is the interpore distance, D_p is the pore diameter and the t_w is the wall thickness

b) Barrier Layer Thickness

Equation 2 states that the anodization voltage is directly proportional to the thickness of the oxide barrier layer (T_b) at the pore bottom. Depending on the anodization regime, the proportional constant (K) has a value of 1,3 for moderate and harsh anodization, respectively. According to the high field conductivity hypothesis, the relationship between current density and barrier layer thickness (T_b) is inverse.

$$T_b = KV$$

Equation 2. T_b is the barrier layer thickness value; K is the proportionally constant and V is the voltage to be applied.

c) Pore Growth Rate

The acid electrolyte temperature has an impact on the pace of pore growth. Since it is directly correlated, the pore growth rate falls as the temperature rises. The temperature must be kept below room temperature, typically at 5°C, to avoid the NAA from dissolving during the anodization process. The pace at which the acid electrolyte is mixed, which ensures the diffusion of ionic species and the homogeneity of the temperature inside the pores, is another factor that affects the rate at which pores expand.

2 Nanoporous Anodic Alumina Fabrication

The experimental techniques for creating nanostructures out of nanoporous anodic alumina are described in this chapter. First, a detailed description and presentation of the electrochemical cell in our facilities. Second, under different electrolyte conditions, the fabrication methods for nanoporous anodic alumina (NAA) are provided. Thirdly, a thorough explanation is given of the manufacturing procedures for inverted funnel-shaped.

2.1 Experimental Setup

The experimental set-up that can be used at our lab facilities comprises of a power supply controlled by a computer, a separate power supply for the electrolyte stirring, and a cooling system to keep the temperature of the anodization cell below ambient temperature.

The copper plate in contact with the anode, where the aluminum sample will be displaced, makes up the anodization cell. A platinum ring set in a Teflon holder that will be submerged in the electrolyte serves as the cathode. A stirrer is also included in this Teflon holder to keep the electrolyte absolutely homogeneous throughout the whole anodization process. To keep the anodization temperature below room temperature, a metal plate in contact with a thermal insulator is positioned beneath the copper plate.

A personal computer is utilized to control the power supply for the anodization process in our research facilities.

2.1.1 Electrochemical Cell

An electrochemical cell is formed with the following parts:

- Anode
- Cathode
- Electrolyte
- Power supply

Because the electrolyte solution serves as a medium for contact between the anode and the cathode, it is necessary for them to be submerged in it. Between the anode and the cathode, the ionic species (H^+ , Al_3^+ , O_2^-) are transported through the electrolyte. The energy required to ionize the aluminum at the aluminum-alumina contact (anode), which generates electrons (e^-), is supplied by the power source. As soon as the anodization voltage is applied, pores begin to form and spread across the aluminum substrate. Figure shows the schematics for an electrochemical cell.

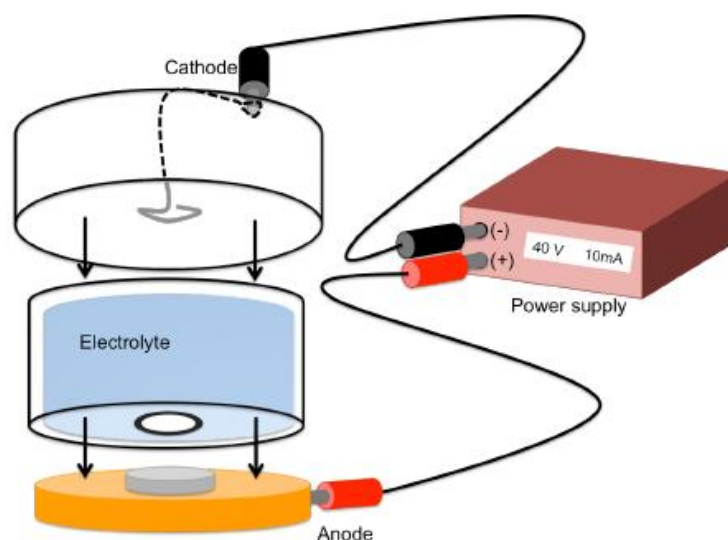


Figure 5. Schematics for the electrochemical anodization cell showing the anode, cathode and the power supply.

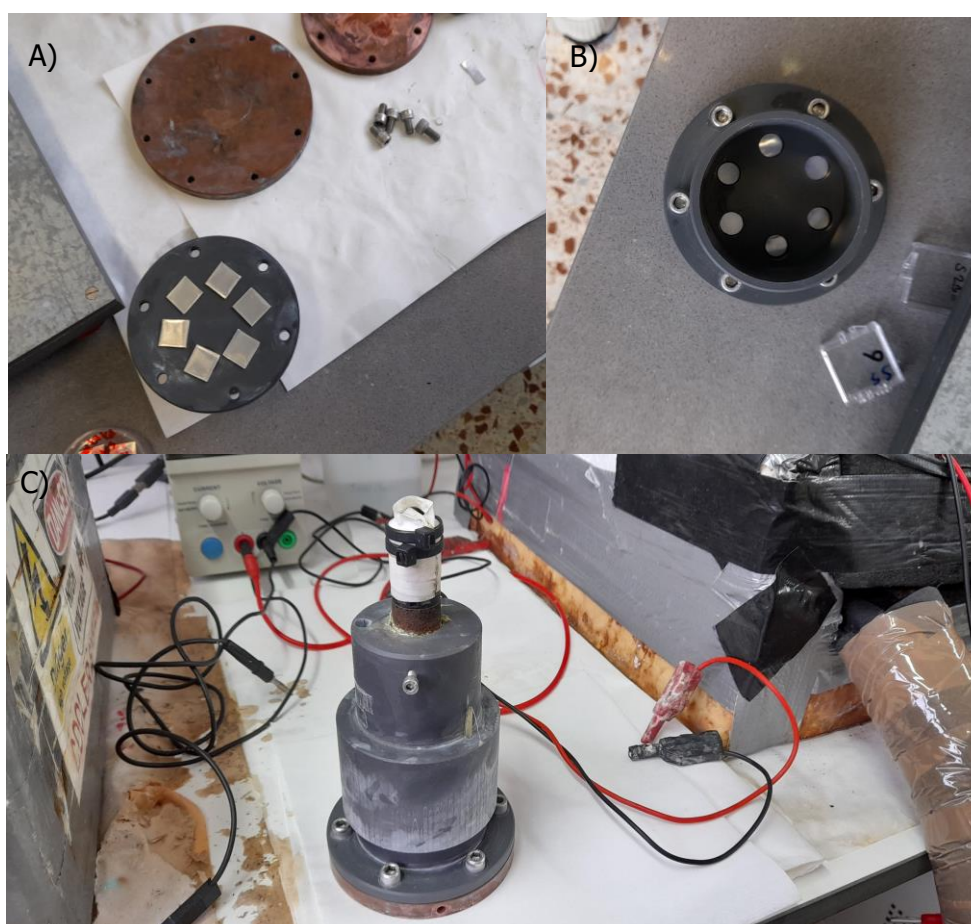


Figure 6. A) Image showing the first step of the chamber assembling where the aluminium samples are displaced on the o-rings. B) The copper base is displaced covering the samples and directly in contact with them and then the screws are assembled. C) Finally the chamber is covered with the cathode and with an isolation hood.

2.1.2 Software

Custom LabView-based tools were used to manage the anodization of aluminum sample samples. A screen shot of a program used to create nanoporous anodic alumina samples is shown in Figure 3s. By altering the voltage and regulating the anodization duration or the total charge traveling through the anodization cell, the sample characteristics can be precisely controlled.

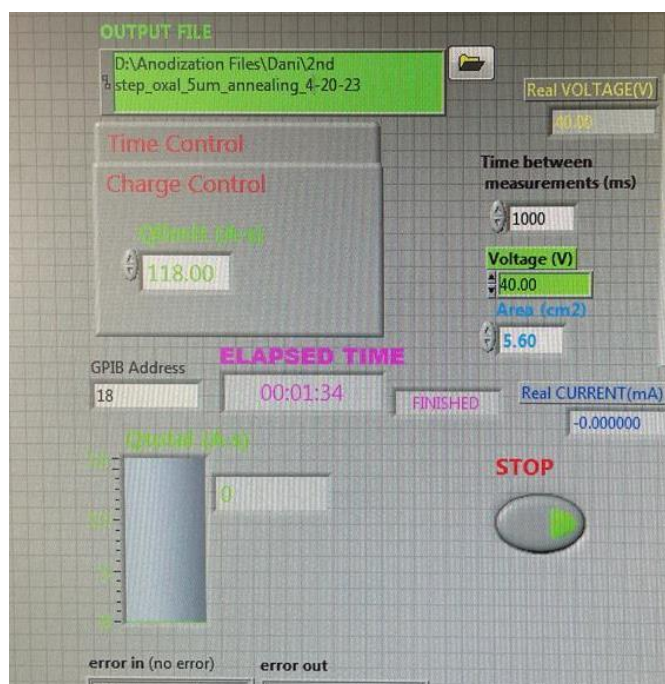


Figure 7. Screen capture of the Lab View based software used in our lab facilities

2.1.3 Aluminium Substrate

Since impurities in the aluminum substrate cause faults in the NAA, high purity aluminum sheets are required in order to produce NAA of a high caliber. High purity aluminum is typically utilized for this reason. The purity of the materials employed in our investigation was 99,999% from Goodfellow.

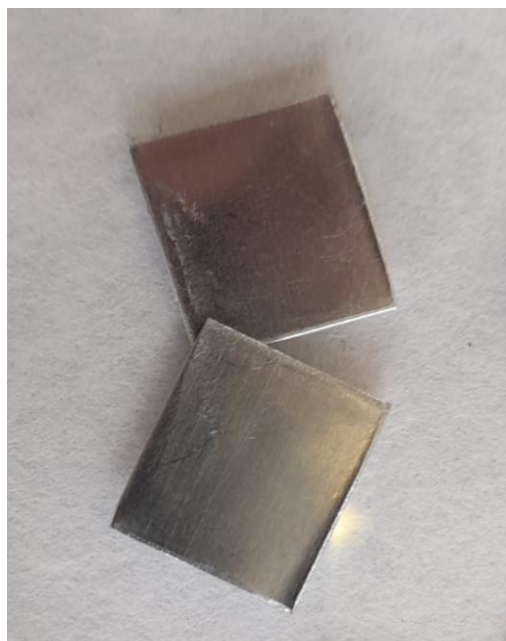


Figure 8. Aluminium foils that were used with 99,999% purity.

2.2 Pre-treatments

The surface of the aluminum substrate will initially already have an oxide layer on it; this layer is often created by atmospheric oxygen. Additionally, a pre-existing surface structure on the substrate may have been created through a mechanical, thermal, chemical, or electrochemical process. All of these surface modifications affect how the pores that will develop on the substrate's surface during the anodization process will self-order. Because of surface flaws like scratches, pits, impurities, and grain boundaries, the pore nucleation process combines random nucleation and nucleation induced by them.

To get rid of any potential surface flaws in the aluminum sample, a common pre-treatment of an aluminum band is required. The pre-treatment starts with electrochemical polishing followed by acetone or a comparable solvent to degrease the foil.

The most well-known method for polishing aluminum foils is electrochemical polishing, or electropolishing. Between its benefits, we can conclude that it is quick and incredibly efficient. The end result has a reflective finish. The most common electrolyte for electropolishing is a 1:4 v:v mixture of perchloric acid and ethanol, which we utilize in our research facilities. Because of the potential of explosion from the heat produced during the electropolishing mixture preparation, it must be done below 0°C.



Figure 9. Electropolished aluminium foils.

2.3 Two-step Anodization

Two-step anodization technique is based on electrochemical oxidation of aluminum foils at modest potentials and potentiostatic circumstances, namely at the breakdown potentials (40 and 197 V for oxalic and phosphoric acids, respectively). By using anodizing settings, this anodization ensures a uniform growth of the oxide layer and good control of the pore size and interpore distance. In this instance, the two-stage anodization procedure is employed to get the right pore ordering. Table 2.1. displays the matching anodization voltages, electrolyte temperatures, and concentrations. The Anodizing potential (Voltage) and the interpore distance (distance between pores) are directly correlated, as shown in **Figure 7**. To produce the greatest hexagonal pore configuration, the initial anodization phase is typically carried out for 20–24 hours. The alumina (Al_2O_3) layer with disordered pores on top and ordered pores at the bottom is disintegrated by wet chemical etching in a mixture of phosphoric acid (H_3PO_4) 0,4M and chromic acid (H_2CrO_7) 0,2M in a volume ratio of 1:1 at 70°C once the initial anodization is complete. Due to the distinctive colour of the specified acid mixture, we dubbed this process "Orange Solution Process". The event lasted two hours. Hemisphere-shaped patterns are now created on the aluminum surface. The second anodization can then be carried out. The required thickness of the alumina layer will determine the duration of the second anodization process. Since we can better manage the layer length this way, total charge is used to regulate the second step anodization rather than time.

Table 2 Anodization parameters of the commonly used acid solutions (oxalic and phosphoric) in mild anodization processes: electrolyte concentration, anodization voltage, electrolyte temperature.

Acid	Concentration	Voltage (V)	Temperature (°C)
H ₂ C ₂ O ₄	0.3M	40	5
H ₃ PO ₄	1 wt%	195	-6

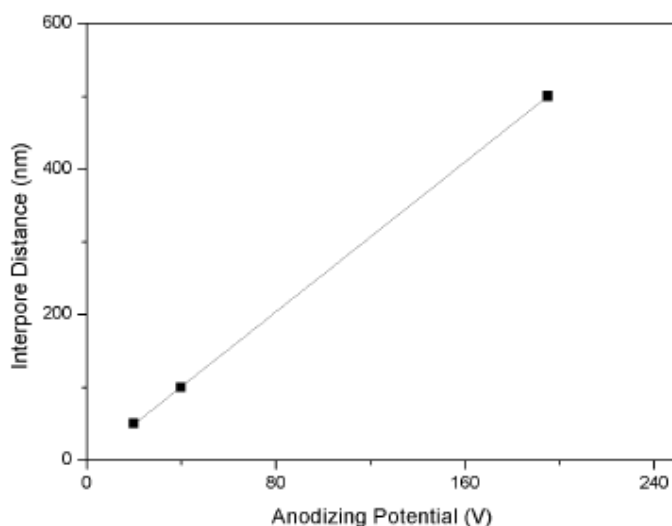


Figure 10. Correlation between interpore distance and the anodizing potential.

a) Two-step anodization by phosphoric acid electrolyte

Aluminum substrates were electropolished for 8 minutes at a constant applied voltage of 20V using a perchloric acid and ethanol (1:3) mixture as the solvent (**Figure 10.A**). Then a protective layer was created at lower voltages (175 V in phosphoric acid for 180 minutes) to inhibit breakdown effects and enable consistent oxide film formation at high voltage (195V in phosphoric acid). The DSM (SM 300-5) SourceMeter was used to monitor and record the voltage and current of the anodization process in this work. A custom computer application based on LabView was used to operate the SourceMeter to have a more exact control of the anodization process.

After completing the pre-anodization at 175 V, a 20-hour ramp at 0,005 V/s was employed to reach the hard anodization voltage (195 V). In order to prevent the current from increasing too quickly and scorching the electrolyte, which would lead to oxide breakdown, the voltage was increased linearly.

The alumina scaffold created by this initial anodization has ordered characteristics at the bottom but has disordered features at the top of the pores (**Figure 10.B**).

After this initial step, the porous alumina that had grown on the aluminum surface was removed using a wet chemical etching process at 70 degrees Celsius with a solution of phosphoric acid (0,4 M) and chromic acid (0,2 M) (1:1 volume ratio). This left a highly periodic structure of nano-concavities that served as the starting points for the formation of pores in the subsequent anodization step.

To create ordered nanoporous alumina, a second anodization was carried out at that point under the same experimental settings (195 V). When pores with a 5 μm depth were attained, the second stage of anodization was applied (**Figure 10.D**).

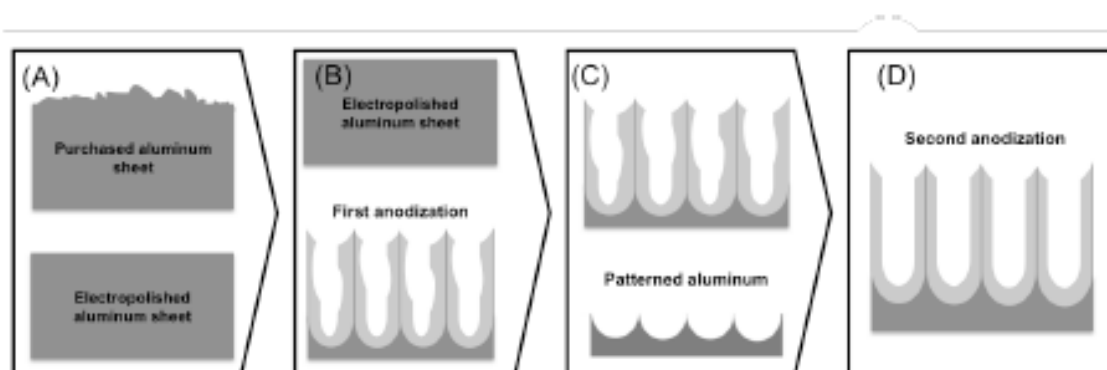


Figure 11. Schematic representation of the alumina pores formation during the anodization process. A) The electropolishing step creates a plane surface. B) The first anodization produces a disordered NAA wall. C) Dissolution of the alumina wall creates an ordered pattern in the aluminum sheet. D) The second anodization on the patterned aluminum creates a perfect ordered NAA.

b) Two-step anodization by oxalic acid electrolyte

A similar procedure was followed using the oxalic acid electrolyte. Using a perchloric acid and ethanol (1:3) mixture as the solvent, aluminum substrates were electropolished for 8 minutes at a constant applied voltage of 20V. We then used our lab software to apply a 40 V for 20 hours to allow a consistent oxide coating to form. This initial anodization produced an alumina scaffold with ordered features at the bottom and disordered features at the top of the pores.

Following this, a wet chemical etching technique at 70 degrees Celsius using a solution of phosphoric acid (0,4 M) and chromic acid (0,2 M) was used to remove the porous alumina that had developed on the aluminum surface.

At that time, a second anodization was performed using the same experimental conditions (40V) to produce ordered nanoporous alumina. The second round of anodization was applied once pores with a 5 μm depth had been established.

c) Calibration Pore Growth

Mild anodization, as mentioned, promotes the growth of homogeneous layers: For this reason, it is possible to imagine that cross section images and the time required to produce them could be used to clarify a calibration curve (**Figure 12**).

Although this calibration curve can provide a good approximation, it has a number of shortcomings: If the sample cross-section photos are not shot perpendicularly and without flaws, inaccurate measurements may be made.

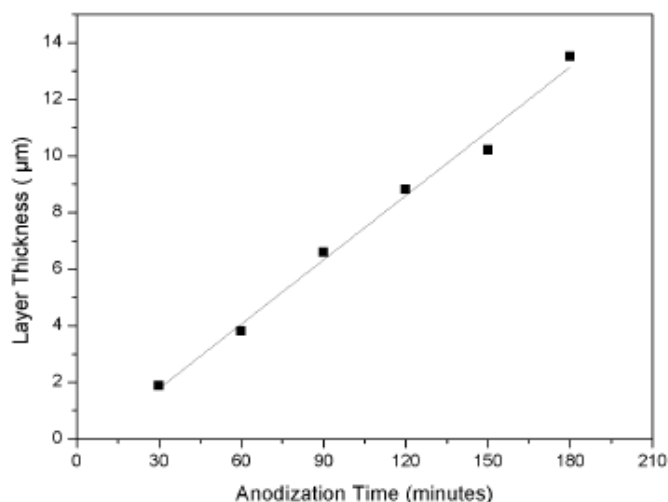


Figure 12. Calibration Curve relating the anodization time (t) and layer thickness (L) for an oxalic acid anodization.

The equation relating the anodization time and layer thickness in the given example (**figure 12**) is the one presented in (**equation 3**):

$$L = (0,0075t) - 0,49$$

Equation 3. Where L is the layer Thickness in nanometers and t is the anodization time in minutes.

A total electrical current charge (Q) calibration has been carried out to predict the developing layer thickness more accurately for all the reasons stated. The anodization of aluminum is primarily controlled by the migration of ionic species to the appropriate electrodes, and the current developed in the electrochemical cell during the anodization process is directly proportional to the amount of alumina generated. This total charge calibration is based on this fact. Because the total charge passed through the electrodes is telling the quantity of NAA generated regardless of the anodization settings, the calibration using total charge is independent of the voltage, electrolyte composition, and temperature. A calibration example is shown in **figure 13**.

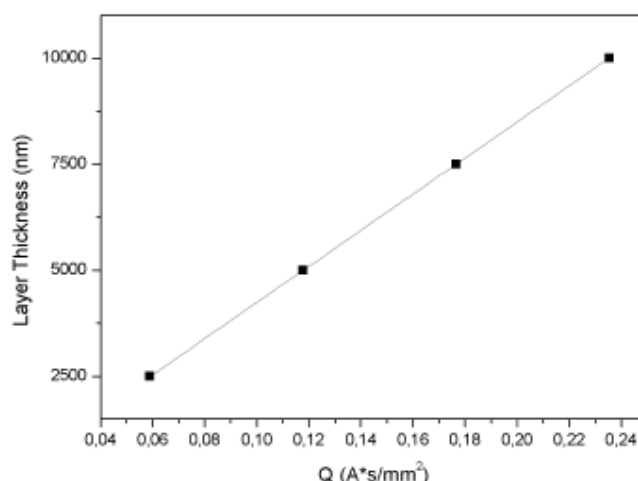


Figure 13. Graph showing the calibration (linear relation) between Q (total charge) and the oxide layer thickness.

The expression to relate the total electric current charge (Q) and the layer thickness is the following equation:

$$Q = \frac{L + 10,877}{42509 * Z}$$

Equation 4. Where Q is the total charge in Amperes per second (A*s), L is the layer thickness in (mm) and Z is the area of the sample anodized in millimetres squared (mm²).

Once the calibration has been completed, a system is utilized to calculate the total electrical current charge (current passed through the system) of the anodization process in real time. When the goal value of Q is reached, the process (anodization) is then terminated.

2.4 Post-treatments

2.4.1 Annealing

The pore walls of aluminum oxide produced by electrochemical anodization are amorphous and polluted with varying concentrations of anions from the acid electrolyte. It has been demonstrated that annealing at a high temperature can transform amorphous oxide membranes into polycrystalline ones. The pore widening procedure is resistant to this crystallization. The resistance to pore expansion and the resistance to crystallization are related. The barrier to pore expansion increases with increasing temperature.

2.4.2 Pore Widening

Wet chemical etching in phosphoric acid is the most popular method for achieving varied porosities in the previously anodized Nanoporous Anodic Alumina. The pore diameter can be controlled effectively using this post-treatment. Additionally, it enables pore diameter to expand without affecting interpore distance. It involves submerging the anodized samples for a predetermined amount of time in a phosphoric acid solution with a 5% weight concentration at 35°C. The pore walls of the aluminum oxide will dissolve in this acid.

It has been demonstrated that the pore diameter will change depending on the voltage used during the anodization process. This is due to the reduced interpore distances and thinner pore walls produced by low voltages. In comparison to pores with wider walls (higher voltages), the porosity will be quickly increased as a result of this reduction by the pore widening post-treatment. Additionally, the electrolyte anions (impurities) that are introduced to the oxide layer have a direct impact on the anodization voltage.

2.5 New Pore Architecture: Inverted Funnel-like Pores

An electrochemical method based on the variation in the dissolving rate of nanoporous anodic alumina with annealing temperature is used to create inverted nanoporous anodic alumina funnels [31].

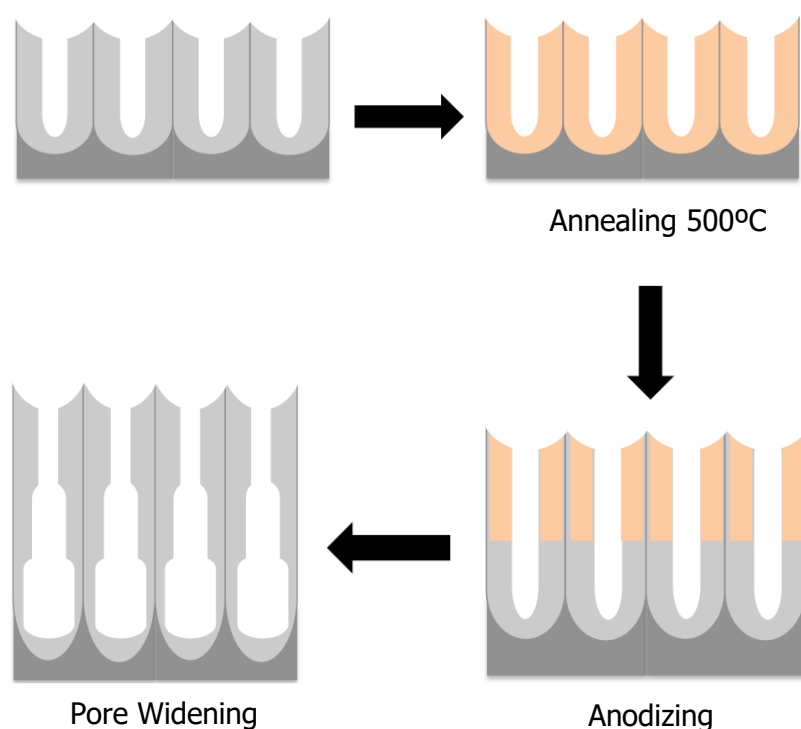


Figure 14. Schematics showing the Inverted funnels fabrication procedure.

Inverted funnels were created utilizing a two-step procedure as it has been described previously. Once the oxalic and phosphoric acid concentrations were 5 μm and 4 μm , respectively, a thermal treatment at 500 $^{\circ}\text{C}$ was carried out for 18 hours. Another anodization was then carried out, this time again with a thickness of between 5 and 4 μm , depending on the acid electrolyte. And eventually, a two-hour pore widening.

Inverted funnels consisted of a top layer of 5 μm , followed by a thermal treatment at 500 $^{\circ}\text{C}$ for 18 hours. A subsequent anodization step added 5 μm thick bottom layer. In a final wet chemical step, the pores were widened for 2 hours.

3 Characterization of NAA structures

All NAA structures were characterized by Field Emission Scanning Electron Microscopy (FESEM, Scios 2 Fei Company).

FESEM, renowned for its exceptional resolution and imaging capabilities, played a pivotal role in our sample analysis. By employing FESEM, we were able to capture high-resolution images that provided a magnified view of the surface features of our samples. The sharpness and clarity of these images were instrumental in accurately assessing the pore diameter, enabling us to analyse the size distribution and morphological characteristics of the pores present in our samples.

To enhance the accuracy of our pore diameter measurements, we employed the widely used ImageJ software. This software is specifically designed for image analysis and provides a range of powerful tools and algorithms to measure various features within digital images. With ImageJ, we were able to precisely measure the pore diameter by selecting regions of interest on the FESEM images and obtaining accurate numerical data.

The utilization of ImageJ software in our study offered several advantages. Firstly, it allowed for automated and systematic measurements, reducing potential human errors and subjectivity. Secondly, it provided a standardized and reproducible approach, ensuring consistency in our measurements across different samples and experiments. Lastly, ImageJ facilitated efficient data analysis by enabling batch processing, thus saving significant time and effort compared to manual measurements.

By combining the high-resolution imaging capabilities of FESEM with the accurate and efficient measurements facilitated by ImageJ software, our study achieved a robust and reliable characterization of the pore diameter in our samples. This comprehensive analysis enhanced our understanding of the samples' structural features.



Figure 15. FESEM microscopy equipment

Drug photoluminescence was used to gauge drug release. The photoluminescence measurements were performed using a fluorescence spectrophotometer from Photon Technology International Inc. (Birmingham, NJ, USA), with a room-temperature Xe lamp

serving as the excitation light source and a 590 nm Xe lamp serving as the emission light source.

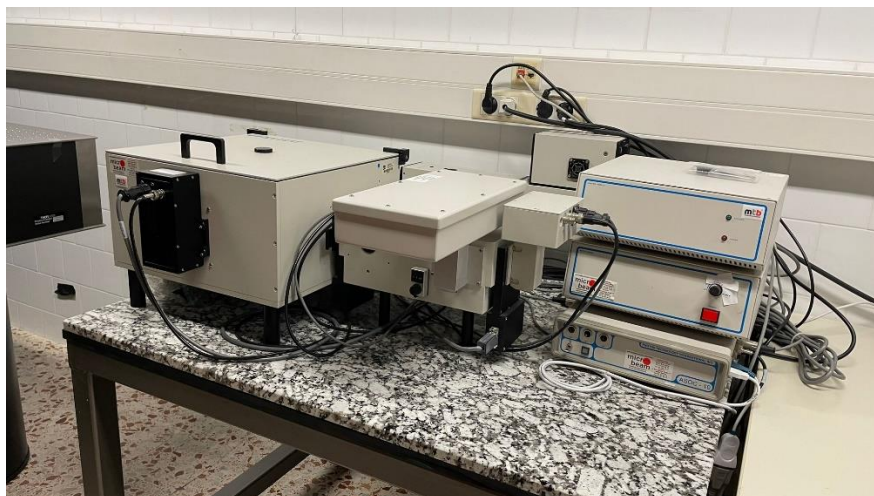


Figure 16. Fluorescence spectrophotometer equipment.

4 Results and Discussion

4.1 Fabrication of Alumina Structures

4.1.1 NAA Structures Using Phosphoric Acid

We will analyse the samples treated with phosphoric acid and observe the expected formation of well-defined pores. The pore diameter remained consistent even when observed from different distances, providing a robust confirmation of their presence. We have determined that the average pore diameter is approximately 120 nanometers.

The samples treated with phosphoric acid exhibited remarkable pore formation, aligning with our expectations. The use of this particular treatment method proved successful in generating well-defined pores with consistent dimensions throughout the sample. Even when observing the samples from varying distances, the pores remained visibly prominent, further affirming their structural integrity and size (**figure 17**).

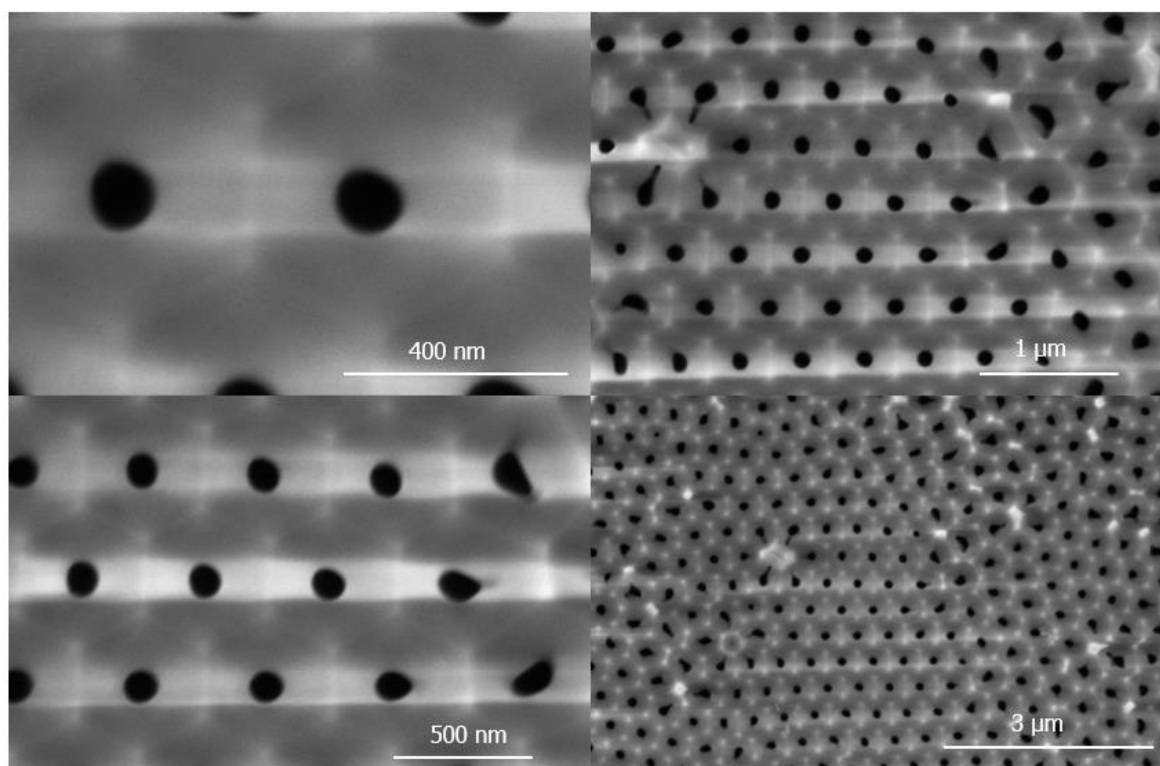


Figure 17. Top View FESEM images of NAA fabrication from Phosphoric Acid

The obtained results reveal a remarkable level of uniformity in the pore distribution, and the observed thickness of the pores closely corresponds to the expected theoretical value of $5\mu\text{m}$ (**figure 18**).

The uniformity of the pores is clearly evident, with consistent pore sizes and distribution observed throughout the cross-sectional area. This visual confirmation of pore uniformity highlights the effectiveness of the phosphoric acid treatment in creating well-defined and evenly distributed pores.

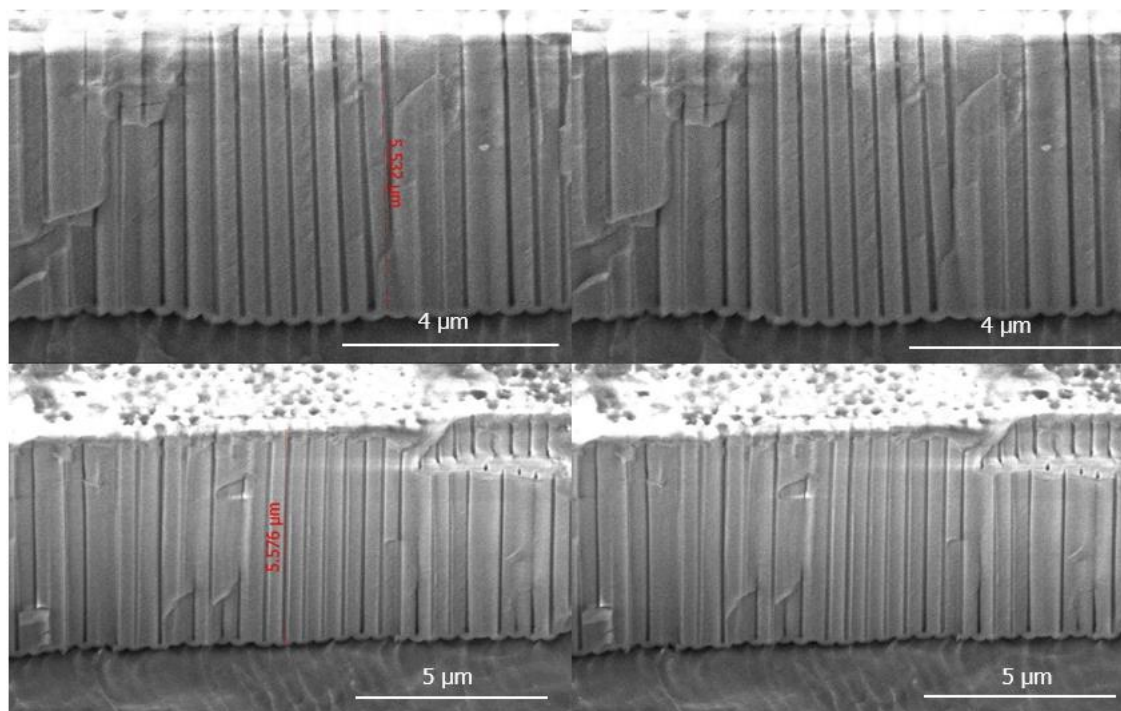


Figure 18. Cross Section FESEM images of NAA fabricated from Phosphoric Acid

Phosphoric acid is known for its aggressive etching action, which can lead to the removal of surface layers and the creation of a rougher texture. As a result, the samples treated with phosphoric acid may lose their mirror-like appearance (**figure 19**) and exhibit a more textured surface. The acid attacks the surface of the material, causing micro-scale irregularities and etch pits that scatter light, leading to a loss of the reflective properties [32].

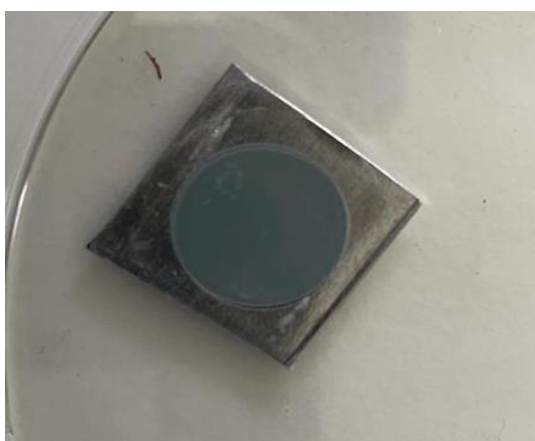


Figure 19. Result of a NAA sample made with phosphoric acid

4.1.2 NAA structures Using Oxalic Acid

In the subsequent stage of our study, we shifted our focus to the samples treated with oxalic acid. The main objective was to investigate the pore characteristics arising from this acid. Notably, we observed that the pores formed using oxalic acid were significantly smaller

in size compared to those induced by phosphoric acid. This discrepancy can be attributed to the distinct chemical nature of oxalic acid.

After surface characterization we found that the average pore diameter in the oxalic acid-treated samples was approximately 30 nm (**figure 20**). This significant reduction in pore size compared to the phosphoric acid-treated samples can be attributed to the differing properties of oxalic acid, which promotes a more controlled and restricted pore growth.

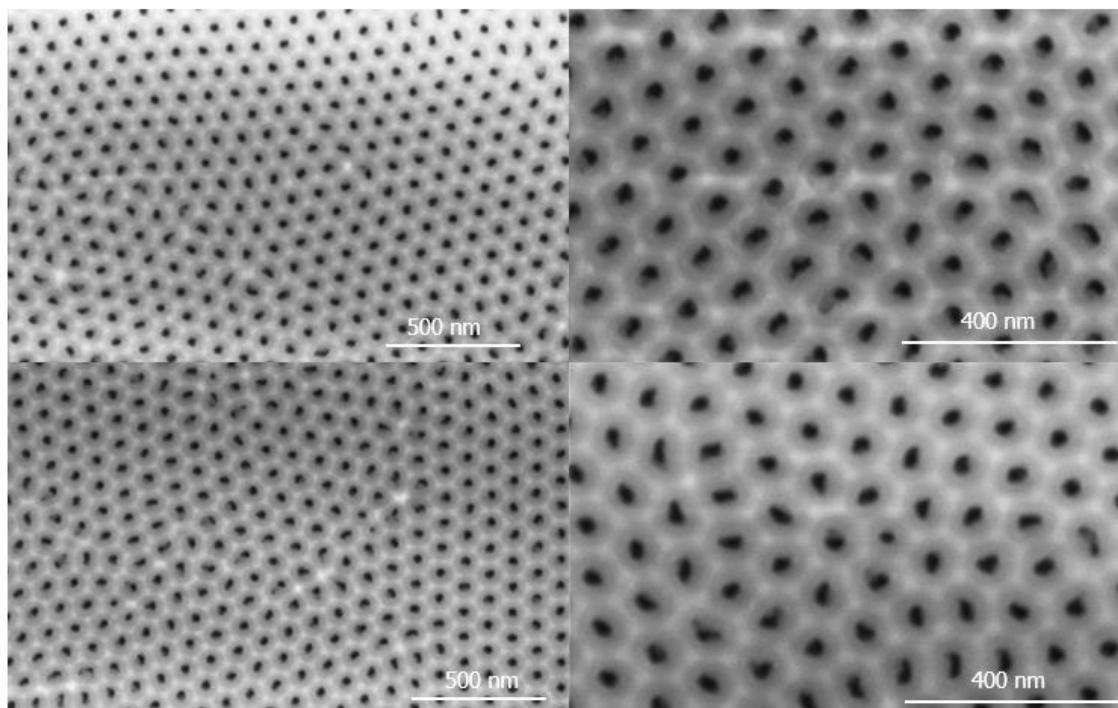


Figure 20. Top view FESEM images of NAA fabricated from oxalic acid.

The cross sections clearly illustrate that the diameters of the pores in the oxalic acid-treated samples are significantly smaller compared to those treated with phosphoric acid. Despite their reduced size, the enhanced uniformity of the pore distribution becomes more pronounced in these cross sections. The smaller pore diameters, coupled with the observed uniformity, provide valuable insights into the impact of the etching method on pore size control and uniformity.

The characterization of cross sections in the oxalic acid-treated samples reveals their unique structural properties (**figure 21**). The close approximation of the observed thickness to the theoretical thickness, combined with the smaller pore diameters and improved uniformity, highlights the effectiveness of the oxalic acid treatment in creating well-defined and consistently sized pores.

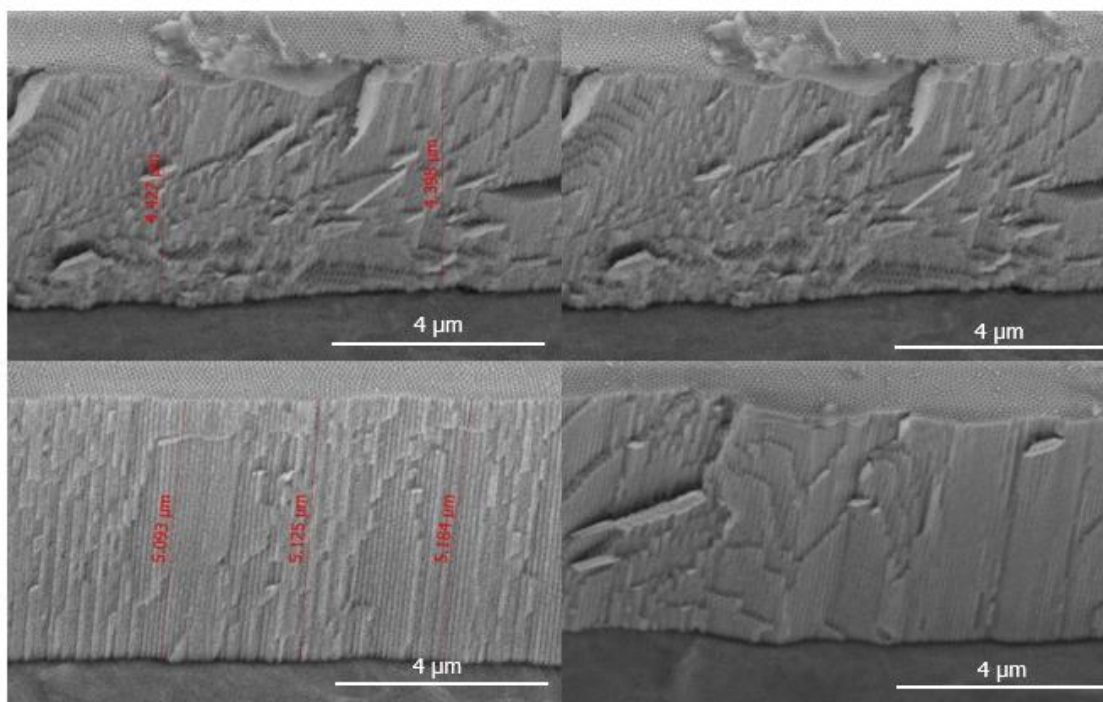


Figure 21. Cross Section FESEM images of NAA fabricated from Oxalic Acid

Oxalic acid typically exhibits a milder etching action compared to phosphoric acid. It selectively removes the surface layers while maintaining a smoother surface texture. The smoother surface allows for better light reflection, preserving the mirror-like appearance of the samples (**figure 22**) [33].

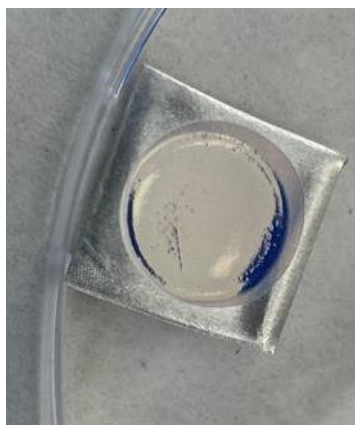


Figure 22. Result of a NAA sample made with oxalic acid

4.1.3 Inverted Funnel Structures

- **IF Fabricated from Phosphoric Acid**

To achieve the desired Inverted Funnel (IF) structures, a thermal treatment was employed to induce a transformation in the alumina's crystallographic phase from amorphous to gamma phase. The temperature utilized for this treatment was set at 500°C. Subsequently, a third round of anodization was performed, resulting in a thickness of 5μm (**figure 14**).

Following this procedure, a pore widening process was conducted for two different times: one hour (**Figure 23**) and two hours (**Figure 24**).

This way, IF had different layers of 5 μm each: an upper one that was treated with 500°C, and for that reason had the narrower pores and, the layer in the bottom that did not receive any temperature treatment reason why had the wider pores.

When alumina is subjected to high temperatures, such as 500°C, it undergoes crystallographic phase transformation. In this case, the amorphous phase is converted to the gamma phase. This phase transformation leads to a more ordered arrangement of atoms within the alumina structure [34].

The increased order and crystallinity of the gamma phase alumina result in a denser and more compact material compared to the amorphous phase. Consequently, during the subsequent anodization and pore widening etching processes, the upper layer with the gamma phase alumina exhibits a more restricted pore growth. The narrower pores in the upper layer can be attributed to the enhanced structural integrity and reduced pore initiation sites, resulting from the thermal treatment.

On the other hand, the lower layer, which did not undergo the thermal treatment, retains the amorphous phase and exhibits wider pores. The absence of the temperature treatment allows for a less ordered atomic arrangement, creating a more porous structure with larger pore sizes.

By incorporating these distinct layers with varying pore sizes, the IF structure is achieved, enabling the desired inverted funnel shape.

The IF structure exhibits a gradient in pore size along its length. Towards the entrance of the funnel, the pores appear narrower, with a diameter of approximately 120 nm. As we progress deeper into the funnel, the pore diameter gradually increases, reaching a maximum value of approximately 270nm in the second half of the pore. Additionally, we observe a corresponding change in the interpore distance. At the entrance of the funnel, the interpore distance measures around 250 nm, while as we go deeper, it decreases to approximately 160 nm. These variations in pore diameter and interpore distance highlight the complex morphological characteristics of the inverted funnel structure.

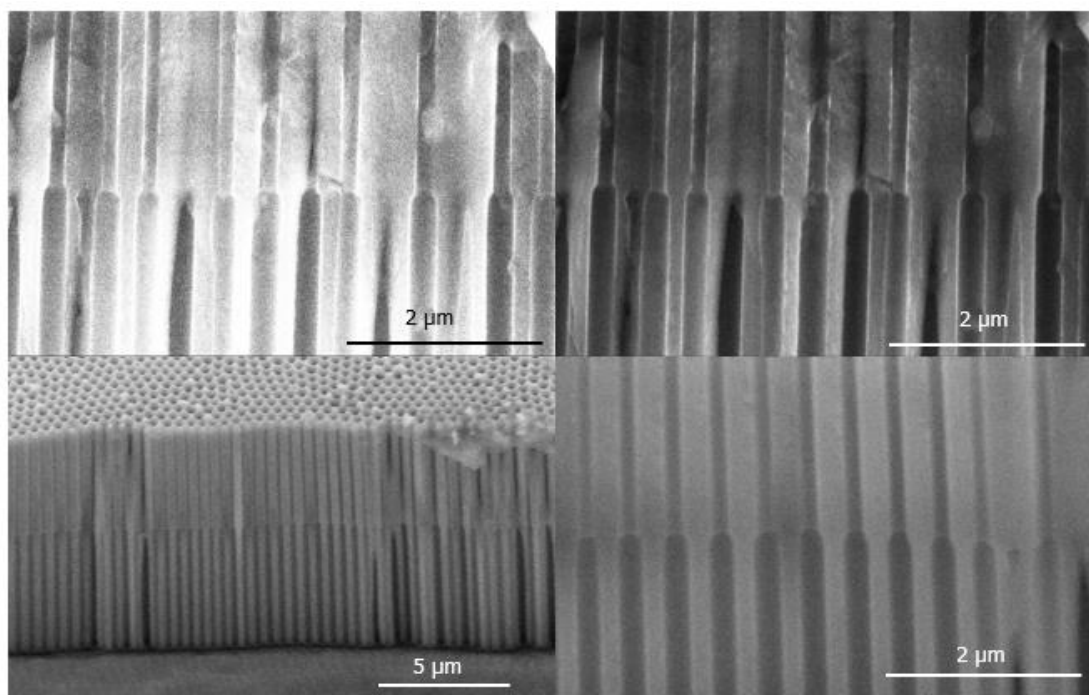


Figure 23. Cross Section FESEM images of NAA IF fabricated from Phosphoric Acid after 1 hour of pore widening.

Continuing our analysis, we shift our attention to the subsequent FESEM image (**Figure 24**), which represents the IF sample subjected to two hours of pore widening.

Here, we observe a further increase in the pore diameter compared to the one-hour sample. The diameter of the pores in this two-hour sample is approximately 400 nm, signifying a substantial expansion in pore size. Interestingly, the interpore distance at the entrance of the funnel remains consistent at around 250 nm. However, as we go deeper into the funnel, the interpore distance decreases significantly to approximately 50 nm. This decrease in interpore distance indicates a higher packing density of pores in the deeper regions of the inverted funnel structure.

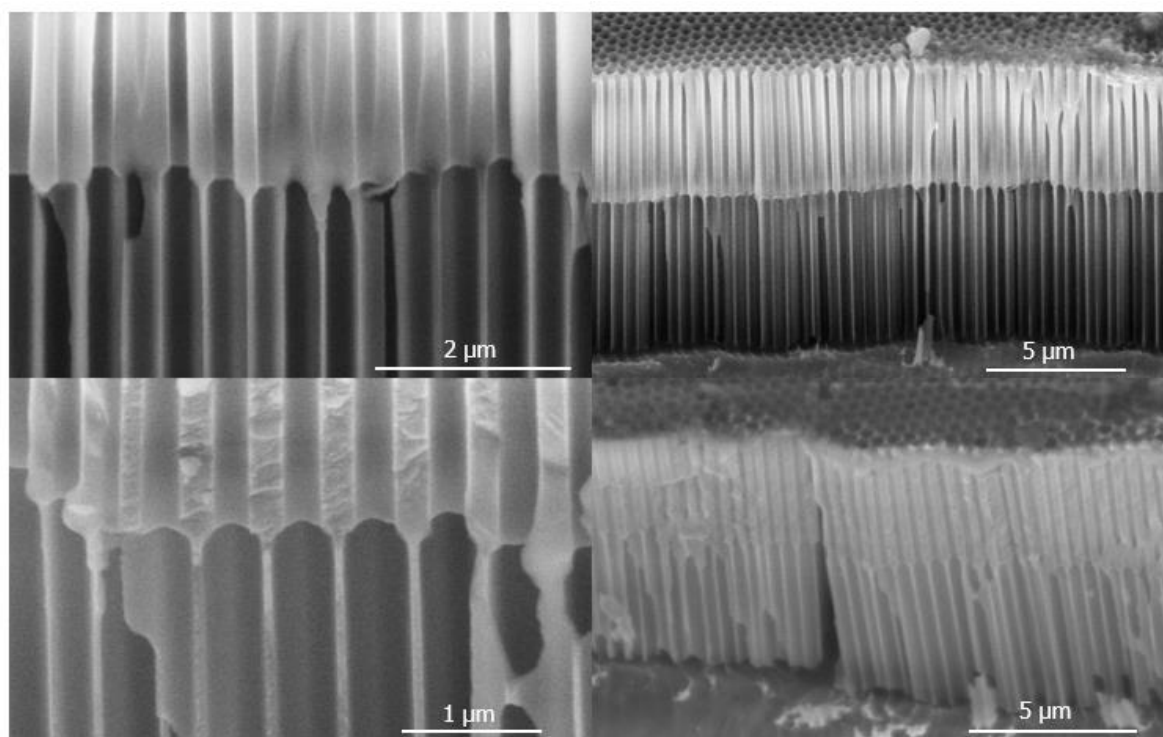


Figure 24. Cross Section FESEM images of NAA IF fabricated from Phosphoric Acid after 2 hours of pore widening.

Comparing the one-hour and two-hour samples, it is evident that the duration of the pore widening process directly impacts both pore size and interpore distance. The one-hour sample demonstrates moderate pore widening, with a corresponding change in interpore distance. On the other hand, the two-hour sample exhibits significantly larger pores and a more pronounced decrease in interpore distance as we move deeper into the funnel.

These observations highlight the intricate relationship between etching time, pore size, and interpore distance in the fabrication of inverted funnel structures. Controlling these parameters is crucial for tailoring the morphology and pore characteristics to meet specific requirements and optimize the performance of the resulting structures.

- **IF fabricated from Oxalic Acid**

In the subsequent part of our analysis, we shift our focus to the inverted funnel (IF) sample formed using oxalic acid as the electrolyte. **Figure 25** illustrates we examine the FESEM image of the IF sample after 40 minutes pore widening

It is challenging to discern any noticeable changes or widening of the pore structure. The image alone does not provide definitive evidence of pore enlargement. However, to gain further insights into the pore morphology, we employed image analysis software, specifically ImageJ, to perform quantitative measurements.

When comparing the pore diameter in the second half of the pore to the first part of the funnel, we observed an increase from approximately 30 nm to approximately 60 nm. Additionally, we also observed changes in the interpore distance along the funnel. At the entrance of the funnel, the interpore distance measured approximately 70 nm, while as we progressed deeper, it decreased to approximately 30 nm.

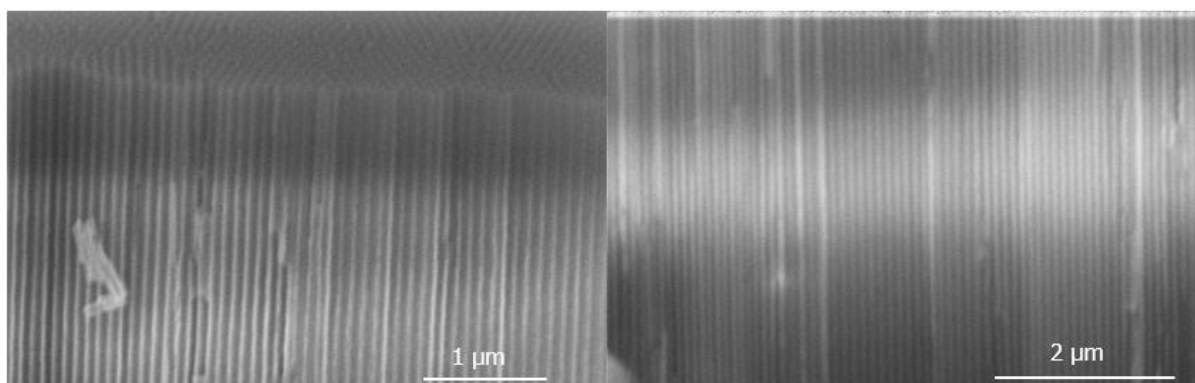


Figure 25. Cross Section FESEM images of NAA IF fabricated from Oxalic Acid after 40 minutes of pore widening.

The disparity in the observed changes between the oxalic acid-formed and phosphoric acid-formed IF samples can be attributed to the inherent differences in the etching characteristics of the two electrolytes. Oxalic acid typically exhibits a slower etching rate and a milder etching action compared to phosphoric acid. This difference in etching behavior leads to a more gradual pore widening effect in the oxalic acid-formed samples.

The differences in pore diameter and interpore distance between the oxalic acid-formed and phosphoric acid-formed IF samples highlight the influence of the choice of electrolyte on the resulting pore morphology. While oxalic acid resulted in more subtle changes, phosphoric acid exhibited a more substantial impact on pore dimensions and interpore distance.

Our analysis reveals that the IF sample formed with oxalic acid experienced a modest widening of the pore diameter and changes in interpore distance, compared to the phosphoric acid-formed samples. These findings emphasize the need for meticulous characterization and fine-tuning of the fabrication processes, including the choice of electrolyte and other process parameters, to achieve the desired pore dimensions and morphology in inverted funnel structures.

4.2 Drug Release Based of Nanoporous Anodic Alumina

4.2.1 Drug Loading

Our study was focused on utilizing NAA structures as the model porous material. These structures offer unique properties that make them ideal for various applications, such as drug delivery.

As a model drug, doxorubicin (DOX), a medication that self-fluoresces, was chosen. It is a well-known and powerful anti-cancer drug used to treat a variety of human ailments.

For the release studies, templates were loaded with a 1 mg/ml concentration of DOX solution in PBS (phosphate buffered saline). The samples were submerged in the suspension and swirled in the dark all night. To maintain the stability of the medicine during the immersion process, the dark atmosphere was maintained to prevent photodegradation of the DOX molecules (**figure 26**).

The choice of DOX for photoluminescence testing is driven by several factors. First, DOX exhibits inherent fluorescence properties, making it suitable for studying light emission phenomena. Its fluorescence behaviour allows for the sensitive detection and quantification of drug diffusion and release within the NAA structures. Additionally, DOX is known for its strong affinity for the nanopore structures. These characteristics enable us to explore the drug's interactions with the nanoporous material and assess its potential as a drug delivery system.



Figure 26. Mounting of the NAA samples dipped in 1 mg/ml of DOX solution on the stirrer overnight.

Following the incubation period, the samples underwent a thorough washing step with deionized water. It helps remove any excess DOX molecules that may be present on the surface of the NAA structures, ensuring accurate and reliable measurements during subsequent analyses. Secondly, it aids in the removal of any residual impurities or byproducts

that could interfere with the photoluminescence testing and adversely affect the overall experimental results.

By carefully controlling the immersion and washing procedures, we can ensure the successful impregnation of DOX into the nanopore material while minimizing the presence of external factors that could confound our photoluminescence analysis. This meticulous approach enables us to investigate the drug release behaviour and assess the efficacy of the NAA scaffold as a potential drug delivery platform[35].

4.2.2 Drug Release

The release studies were performed in vitro using phosphate-buffered saline (PBS), which is commonly employed to simulate in vivo conditions for drug release. Dox was measured directly in the release medium. This design is critical to understand the release kinetics since it allows the collection of fast and frequent data over time. One of the advantages of the in-situ measurement setup used in these experiments is that it is possible to collect release data frequently, which helps in understanding the short-term burst effect.

To evaluate the release behaviour, we conducted release trials where the diffusion of DOX in PBS was monitored over time. This allowed us to examine the release characteristics of the drug respect to the type of acid electrolyte used in the NAA fabrication and the pore shape of the structure.

To establish a relationship between the photoluminescence values and the concentration of DOX, a calibration curve was constructed. This curve allowed us to accurately determine the concentration of DOX based on the photoluminescence readings obtained from the fluorescence spectrometer. The calibration curve was generated by measuring the photoluminescence intensity of known concentrations of DOX under the same experimental conditions used for the release trials.

In order to generate a calibration curve, we performed photoluminescence measurements on various concentrations of DOX. Initially, we prepared solutions with concentrations of 0.1 mg/ml, 0.001 mg/ml, 0.01 mg/ml, and 0.0001 mg/ml. However, during the measurement process, we observed that the photoluminescence (PL) values exhibited oscillations between the 0.01 mg/ml and 0.001 mg/ml concentrations.

To obtain a more accurate calibration curve, we decided to evaluate additional specific concentrations of DOX. Specifically, we included concentrations of 0.0025 mg/ml, 0.005 mg/ml, and 0.0075 mg/ml in our analysis (**figure 27**). By expanding the concentration range, we aimed to capture a more comprehensive representation of the relationship between photoluminescence intensity and DOX concentration.

This adjustment in the concentration range allowed us to obtain a calibration curve that better reflected the response of the photoluminescence measurements to varying DOX concentrations. Consequently, we could establish a more precise relationship between the photoluminescence values obtained from the release trials and the corresponding concentrations of DOX released from the NAA samples.

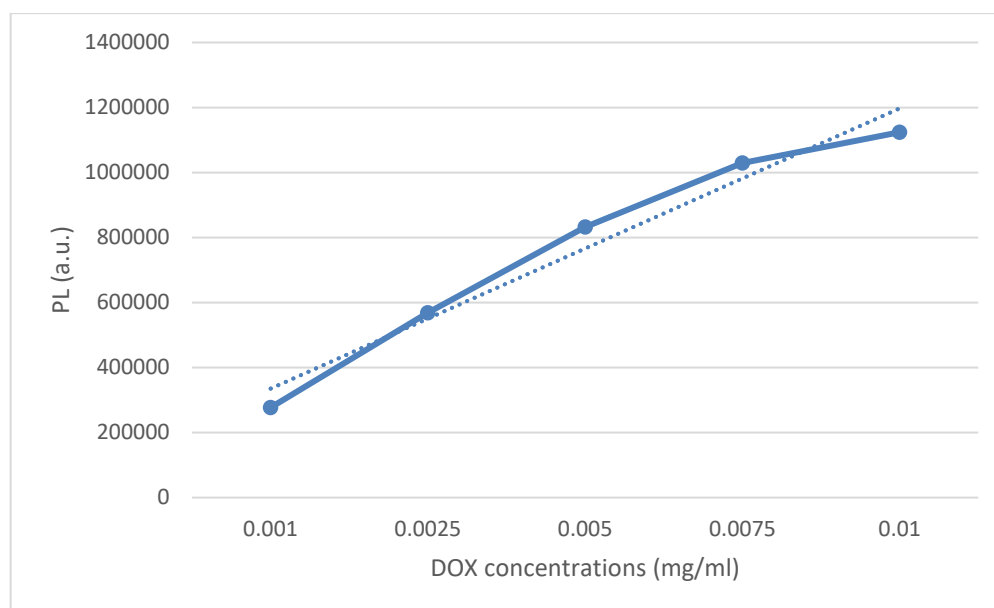


Figure 27. Calibration curve for different Doxorubicin concentrations and their Photoluminescence values.

The aim of this work is to study the effect of pore geometry on the short-term (1440 minutes) release of DOX across all the fabricated NAA structures.

By meticulously studying the interplay between pore shape, size, and distribution, we gain crucial insights into how these geometric parameters affect the release kinetics and performance of the drug delivery system. This comprehensive analysis allows us to unravel the intricate relationship between pore geometry and the efficiency of drug release, shedding light on the fundamental principles that govern drug transport within the NAA scaffolds.

The combination of photoluminescence measurements, time-dependent monitoring, and the calibration curve allowed us to accurately quantify the release of DOX from the NAA scaffolds. This comprehensive analysis facilitated the characterization of the drug release profile and provided valuable information on the controlled release capabilities of the NAA scaffold system.

By analysing the release profiles and comparing the calculated amounts of DOX for each sample, we gained insights into the release kinetics and performance of the NAA scaffolds. This approach allowed us to assess the efficiency of drug release from the different samples and determine any variations or trends in their release behaviour.

In **Figure 28** a release profile is shown for NAA monolayers (straight pores).

NAA monolayer samples fabricated from phosphoric acid exhibit a larger pore size compared to those formed with oxalic acid. This disparity in pore size directly influences the amount of drug that can be loaded within the samples. The larger pore size of the phosphoric acid samples allows for a higher drug-loading capacity, resulting in a greater quantity of drug being released over time. This confirms the crucial role of pore size as a key determinant of drug release, with larger pores facilitating a higher drug release.

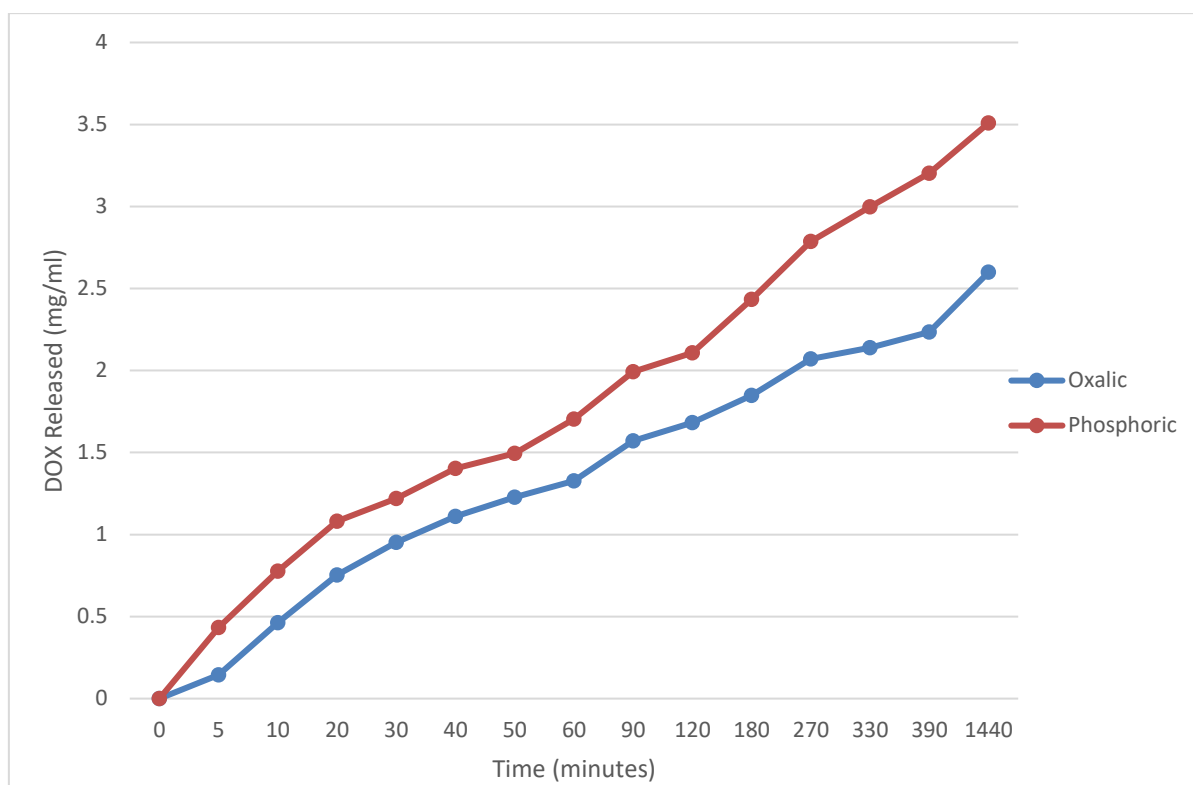


Figure 28. Drug Release of NAA monolayers.

However, what is particularly interesting in this comparison is the similarity in release patterns between the monolayer samples formed with both acids. Despite the disparity in pore size, the release kinetics remain consistent, indicating that the specific shape of the monolayer pore structure plays a dominant role in governing the release rate of the drug. This finding suggests that the geometrical characteristics of the pore shape, such as its surface area and geometry, exert a substantial influence on the diffusion and release of the drug molecules. The similarity in release patterns between the two monolayer samples underscores the importance of considering pore shape alongside pore size when designing drug delivery systems.

When comparing the three inverted funnel samples, it is evident that the phosphoric acid samples exhibit a similar release pattern, while the oxalic acid sample shows a different behaviour. This discrepancy can be attributed to the observations made earlier regarding pore widening (**figure 29**).

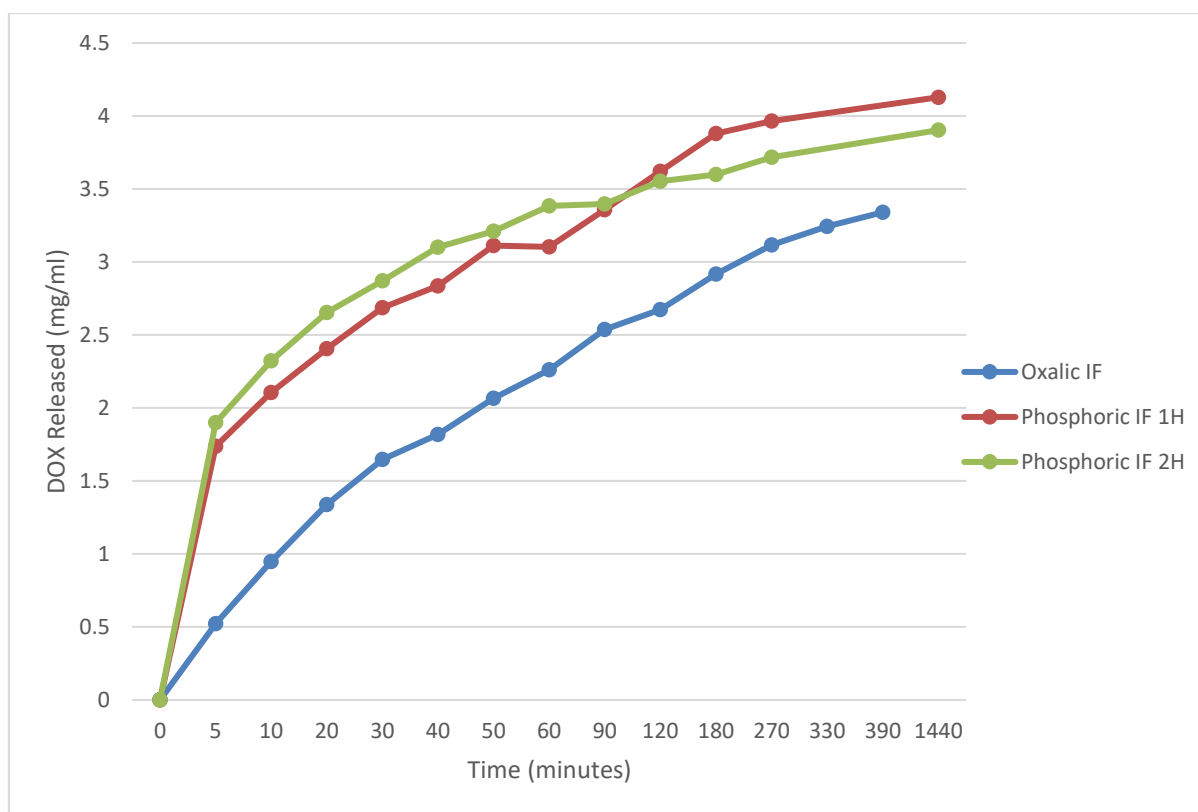


Figure 29. Drug Release of Inverted Funnel Structures of NAA

As previously discussed, the phosphoric acid inverted funnel samples underwent noticeable pore widening, resulting in a larger pore size. This enlargement allows for a more significant amount of drug to be loaded into the pores, leading to a relatively consistent and sustained release pattern. Additionally, it is worth noting that in the initial 5 minutes of release, the phosphoric acid inverted funnels exhibited a release rate nearly three times faster compared to the oxalic acid inverted funnels.

On the other hand, the oxalic acid inverted funnel sample did not experience substantial pore widening. As a result, the pore size remained relatively smaller compared to the phosphoric acid samples. This difference in pore size directly affects the drug loading capacity, resulting in a lower amount of drug being loaded into the pores of the oxalic acid sample.

Consequently, the release pattern of the oxalic acid inverted funnel sample differs from that of the phosphoric acid samples. The limited drug loading capacity in the smaller pores of the oxalic acid sample may result in a faster initial release of the drug. However, as the drug concentration decreases within the limited pore space, the release rate may slow down, leading to a distinct release pattern compared to the phosphoric acid samples.

Figure 30 shows the release profiles of the three different samples fabricated by phosphoric acid: the monolayer, the inverted funnel sample after 1 hour of pore widening, and the inverted funnel sample after 2 hours of pore widening. Our aim is to gain a deeper understanding of how these variations in sample structure and etching time influence the release behaviour of DOX.

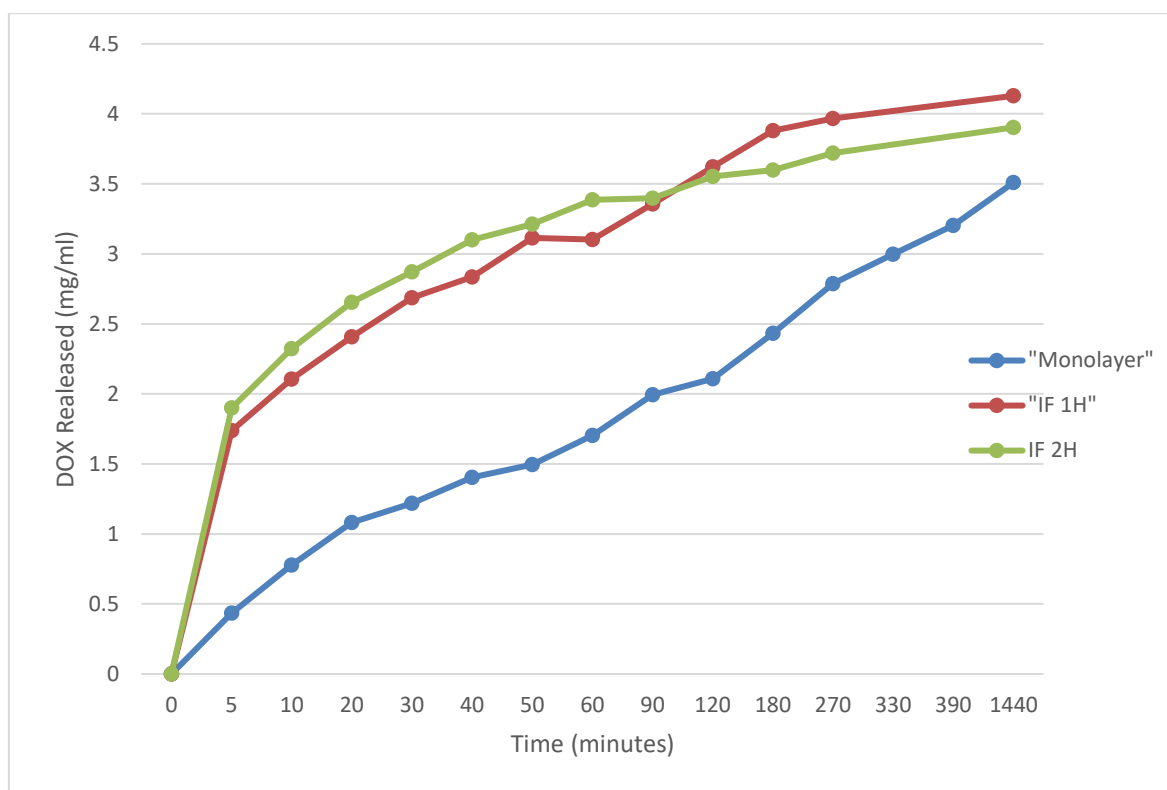


Figure 30. Drug release of NAA structures fabricated by phosphoric acid.

Upon careful examination, it becomes evident that both of the inverted funnel samples exhibit a significantly higher release of DOX compared to the monolayer sample. This disparity can be attributed to the distinctive pore characteristics present in each sample. The inverted funnel samples possess larger pore areas, allowing for a greater quantity of DOX to be loaded into the scaffold and subsequently released over time. In contrast, the monolayer sample, with its relatively smaller pore area, exhibits a comparatively lower release of DOX.

Further analysis of the inverted funnel samples reveals interesting insights into their release profiles. The inverted funnel structure after 1 hour of pore widening displays a relatively more continuous release pattern. This sample demonstrates a gradual and sustained release of DOX, steadily increasing the concentration over time until it reaches a plateau at approximately 4 mg/ml. This sustained release behavior suggests that the pore structure of the inverted funnel allows for a controlled and sustained diffusion of DOX, resulting in a more prolonged release profile.

On the other hand, the inverted funnel structure after 2 hours of pore widening exhibits a distinct release pattern. Initially, this sample shows a rapid release of DOX, indicating a more pronounced burst release phenomenon. However, as the concentration of DOX reaches approximately 3.75 mg/ml, the release rate begins to slow down considerably. This observation suggests that the sample with 2 hours of pore widening has resulted in a structure that offers initial high permeability, facilitating a rapid release of DOX. However, once the concentration threshold is reached, the diffusion rate decreases, leading to a slower release thereafter. This behaviour might be attributed to the changes in pore geometry and pore connectivity induced by the longer widening time.

In comparison, the monolayer sample exhibits a consistent and continuous release profile throughout the monitoring period. The release rate remains relatively constant, indicating a uniform and predictable diffusion of DOX from the NAA sample. The monolayer

structure, with its relatively uniform pore size and shape, ensures a steady release of DOX without significant fluctuations.

Through this comparative analysis, it is evident that the quantity and velocity of DOX release are influenced by both the size and shape of the pores. Larger pore areas and specific pore geometries, such as the inverted funnel configuration, play a significant role in determining the release behaviour of loaded drugs. The variations observed in the release profiles highlight the importance of tailoring the pore characteristics to achieve desired release kinetics and optimize drug delivery performance.

Figure 31 illustrates the drug release of alumina structures formed using oxalic acid, specifically the monolayer sample and the inverted funnel sample after 40 minutes of pore widening. Our objective is to examine and contrast the release characteristics of these two samples and gain insights into how their structural differences influence the release of DOX.

As expected, we find that the inverted funnel sample exhibits a higher release of DOX compared to the monolayer sample. This disparity can be attributed to the larger pore area present in the inverted funnel structure, which allows for a greater quantity of DOX to be loaded and subsequently released.

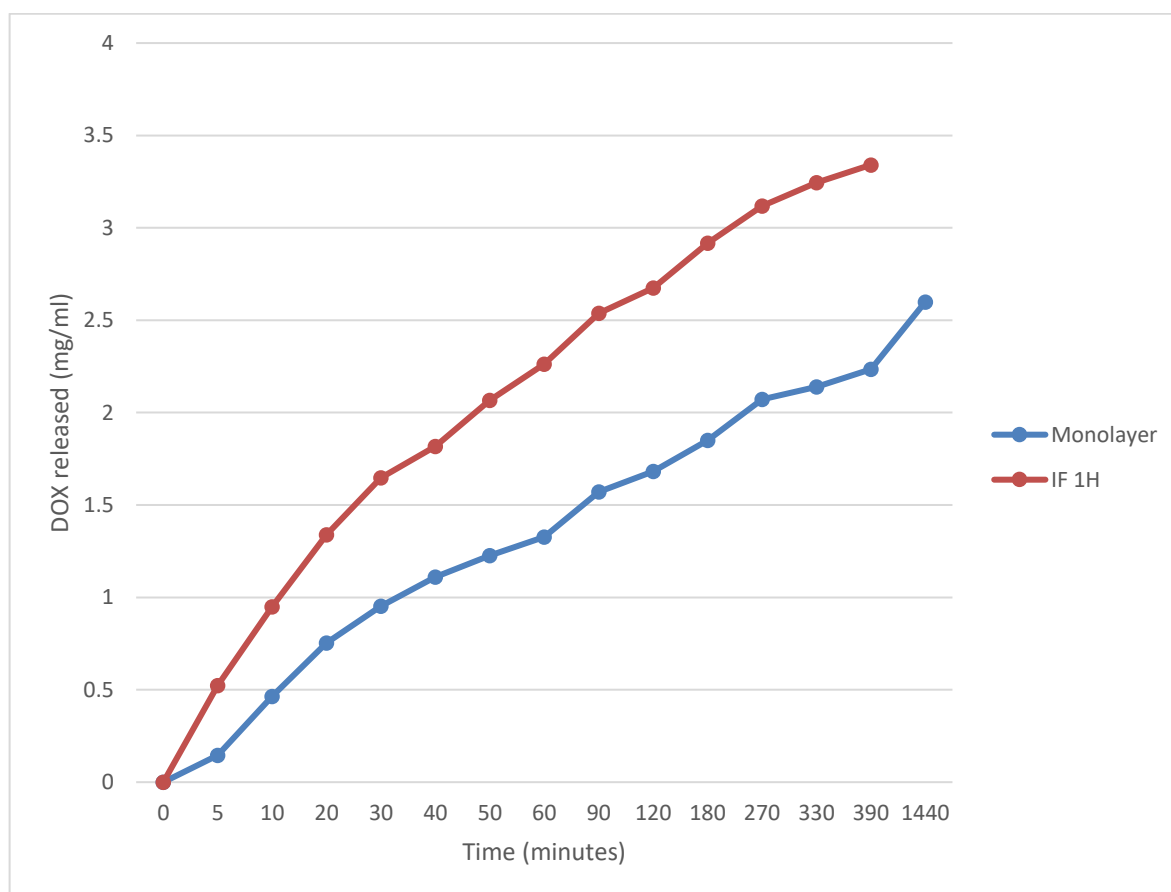


Figure 31. Drug release of NAA structures fabricated by oxalic acid.

Upon closer analysis, we observe that both the monolayer and inverted funnel samples demonstrate a continuous release of DOX. This indicates that the release of the drug occurs steadily over time, without significant fluctuations or abrupt changes in the release rate. This

sustained release behavior suggests that the structural features of both samples, such as the pore size and shape, facilitate a controlled diffusion of DOX from the NAA samples.

Interestingly, the release rates of the monolayer and inverted funnel samples are quite similar, despite the theoretical differences in their pore structures. This observation suggests that factors other than the pore area, such as the specific shape of the inverted funnel, play a role in determining the release rate of DOX. Previous observations made during the analysis of the inverted funnel samples formed using phosphoric acid support this notion. It was noted that the shape of the funnel remained relatively unchanged during the etching process, indicating that the shape itself contributes to the release kinetics of DOX. This consistency in release rate between the monolayer and inverted funnel samples formed with oxalic acid further confirms the impact of the funnel shape on the release behaviour of DOX.

These findings emphasize the significance of pore geometry and shape in dictating the release kinetics of loaded drugs from NAA structure. The results suggest that variations in pore shape can have a considerable influence on the release rate, even in the absence of significant changes in pore area. They don't only confirm our previous observations but also highlight the significance of optimizing both pore size and shape to achieve desired drug release profiles. By tailoring the NAA pore characteristics, researchers can modulate the release kinetics of therapeutic agents, enabling precise control over the delivery of drugs and enhancing therapeutic outcomes.

5 Conclusions

In this graduation thesis, an innovative NAA is presented as a controlled drug release system. Inverted funnel-like structures were obtained using the two-step anodization technique and they were compared with regular pores. This study takes profit of the differences on pore widening rates after temperature treatment of the NAA to create the different structures. With this technology the purpose of the study was to find the best structure for drug release

Our research has yielded valuable insights into the fabrication process and the influence of key parameters on the characteristics of different structures.

A significant aspect of our investigation was the implementation of annealing on the NAA samples. Through this annealing process, we were able to achieve a remarkable advancement in the enlargement of pore thickness. By carefully controlling the annealing conditions, we effectively increased the thickness of the pores, consequently leading to the enlargement of the diameter in the second section of the pores in the funnel's structures.

This capability to control pore dimensions and morphology through annealing has substantial implications for drug delivery applications. The diameter of the pores plays a critical role in regulating the release of drugs from these structures. By enlarging the diameter of the second section of the pores, we have provided a means to fine-tune and optimize drug release kinetics. This level of control over pore dimensions is crucial in designing drug delivery systems that can deliver therapeutics at specific rates and achieve desired therapeutic outcomes.

During the short time release, the inverted funnel structures, which exhibited enlarged pores and controlled pore diameter, show a higher initial release of the drug doxorubicin (DOX) compared to the monolayer structures. However, the inverted funnel structures also displayed a more rapid release rate. However, the monolayer structures exhibited a constant release rate of DOX over time.

These results demonstrate the importance of precise fabrication and design of NAA structures for drug delivery applications. The successful implementation of annealing to enlarge pore thickness and diameter in the second section of the pores highlights the potential for tailoring drug release kinetics. By optimizing the fabrication processes and structure design, we can strive to achieve desired release profiles, providing enhanced control and efficacy in drug delivery systems.

In addition to the existing conclusion, it is important to acknowledge that the results presented in this thesis represent preliminary findings aimed at assessing the functionality of the fabricated NAA structures. As such, the study will be extended to longer release durations to observe the complete release profiles and to explore the performance of new sample designs. These forthcoming investigations will provide a more comprehensive understanding of the drug release behaviour and allow for further optimization of the NAA structures for enhanced drug delivery applications.

In summary, this thesis has contributed to advancing the understanding of NAA fabrication and design, particularly in the context of drug delivery applications. Our utilization of annealing has proven instrumental in enlarging pore thickness and diameter, allowing for greater control over drug release kinetics. These findings lay the foundation for further research and development in the field, with the ultimate aim of improving patient care and advancing pharmaceutical sciences.

6 References

- [1] Hoffman, A.S. (2008) 'The origins and evolution of "controlled" Drug Delivery Systems', *Journal of Controlled Release*, 132(3), pp. 153–63. doi:10.1016/j.jconrel.2008.08.012.
- [2] M. V. Yezhelyev, X. Gao, and Y. Xing, et al., "Emerging use of nanoparticles in diagnosis and treatment of breast cancer," *The Lancet Oncology*, vol. 7, no. 8, pp. 657–667, 2006. doi:10.1016/s1470-2045(06)70793-8
- [3] O. S. Tang, H. Schweer, and H. W. Seyberth, et al., "Pharmacokinetics of different routes of administration of Misoprostol," *Human Reproduction*, vol. 17, no. 2, pp. 332–336, 2002. doi:10.1093/humrep/17.2.332
- [4] K. El-Boghdadly, A. Pawa, and K. J. Chin, "Local anesthetic systemic toxicity: Current perspectives," *Local and Regional Anesthesia*, vol. 11, pp. 35–44, 2018. doi:10.2147/lra.s154512
- [5] G. Price and D. A. Patel, "Drug bioavailability - statpearls - NCBI bookshelf," National Library of Medicine, <https://www.ncbi.nlm.nih.gov/books/NBK557852/> (accessed May 26, 2023).
- [6] S. Adepu and S. Ramakrishna, "Controlled Drug Delivery Systems: Current status and Future Directions," *Molecules*, vol. 26, no. 19, p. 5905, 2021. doi:10.3390/molecules26195905
- [7] C.-C. Lin and A. T. Metters, "Hydrogels in controlled release formulations: Network Design and mathematical modeling," *Advanced Drug Delivery Reviews*, vol. 58, no. 12–13, pp. 1379–1408, 2006. doi:10.1016/j.addr.2006.09.004.
- [8] M. Sinn Aw, M. Kurian, and D. Losic, "Non-eroding drug-releasing implants with ordered nanoporous and nanotubular structures: Concepts for controlling drug release," *Biomater. Sci.*, vol. 2, no. 1, pp. 10–34, 2014. doi:10.1039/c3bm60196j
- [9] [1] D. Losic and S. Simovic, "Self-ordered Nanopore and nanotube platforms for Drug Delivery Applications," *Expert Opinion on Drug Delivery*, vol. 6, no. 12, pp. 1363–1381, 2009. doi:10.1517/17425240903300857
- [10] [10] A. S. Hoffman, "The origins and evolution of 'controlled' Drug Delivery Systems," *Journal of Controlled Release*, vol. 132, no. 3, pp. 153–63, 2008. doi:10.1016/j.jconrel.2008.08.012
- [11] E. Xifre-Perez, S. Guaita-Esteruelas, and M. Baranowska, et al., "In vitro biocompatibility of surface-modified porous alumina particles for hepg2 tumor cells: Toward early diagnosis and targeted treatment," *ACS Applied Materials & Interfaces*, vol. 7, no. 33, pp. 18600–18608, 2015. doi:10.1021/acsami.5b05016
- [12] E. Xifre-Perez, J. Ferre-Borull, J. Pallares, and L. F. Marsal, "Mesoporous alumina as a biomaterial for biomedical applications," *Open Material Sciences*, vol. 2, no. 1, pp. 13–32, 2015. doi:10.1515/mesbi-2015-0004
- [13] S. Simovic, D. Losic, and K. Vasilev, "Controlled drug release from porous materials by plasma polymer deposition," *Chemical Communications*, vol. 46, no. 8, pp. 1317–9, 2010. doi:10.1039/b919840g
- [14] K. Shimizu, K. Kobayashi, G. E. Thompson, and G. C. Wood, "Development of porous anodic films on aluminium," *Philosophical Magazine A*, vol. 66, no. 4, pp. 643–652, 1992. doi:10.1080/01418619208201581
- [15] H. Masuda and K. Fukuda, "Ordered metal nanohole arrays made by a two-step replication of honeycomb structures of anodic alumina," *Science*, vol. 268, no. 5216, pp. 1466–1468, 1995. doi:10.1126/science.268.5216.1466
- [16] A. Santos, T. Kumeria, and D. Losic, "Nanoporous anodic alumina: A versatile platform for optical biosensors," *Materials*, vol. 7, no. 6, pp. 4297–4320, 2014. doi:10.3390/ma7064297
- [17] W. Lee and S.-J. Park, "Porous anodic aluminum oxide: Anodization and templated synthesis of functional nanostructures," *Chemical Reviews*, vol. 114, no. 15, pp. 7487–7556, 2014. doi:10.1021/cr500002z
- [18] L. Yi, L. Zhiyuan, and H. Xing, et al., "Investigation of intrinsic mechanisms of aluminium anodization processes by analyzing the current density," *RSC Advances*, vol. 2, no. 12, p. 5164, 2012. doi:10.1039/c2ra01050j

- [19] V. P. Parkhutik, "Modelling of low-temperature oxidation of materials in gaseous environments," *Journal of Physics D: Applied Physics*, vol. 25, no. 2, pp. 256–261, 1992. doi:10.1088/0022-3727/25/2/019
- [20] G. E. Thompson, "Porous anodic alumina: Fabrication, characterization and applications," *Thin Solid Films*, vol. 297, no. 1–2, pp. 192–201, 1997. doi:10.1016/s0040-6090(96)09440-0
- [21] G. E. Thompson, Y. Xu, and P. Skeldon, et al., "Anodic oxidation of aluminium," *Philosophical Magazine B*, vol. 55, no. 6, pp. 651–667, 1987. doi:10.1080/13642818708218371
- [22] F. Li, L. Zhang, and R. M. Metzger, "On the growth of highly ordered pores in anodized aluminum oxide," *Chemistry of Materials*, vol. 10, no. 9, pp. 2470–2480, 1998. doi:10.1021/cm980163a
- [23] J. M. Montero Moreno, M. Waleczek, and S. Martens, et al., "Constrained Order in nanoporous alumina with high aspect ratio: Smart combination of interference lithography and hard anodization," *Advanced Functional Materials*, vol. 24, no. 13, pp. 1857–1863, 2013. doi:10.1002/adfm.201303268
- [24] F. Keller, M. S. Hunter, and D. L. Robinson, "Structural features of oxide coatings on aluminum," *Journal of The Electrochemical Society*, vol. 100, no. 9, p. 411, 1953. doi:10.1149/1.2781142
- [25] K. Nielsch, J. Choi, and K. Schwirn, et al., "Self-ordering regimes of porous alumina: the 10 porosity rule," *Nano Letters*, vol. 2, no. 7, pp. 677–680, 2002. doi:10.1021/nl025537k
- [26] H. Masuda, H. Yamada, and M. Satoh, et al., "Highly ordered nanochannel-array architecture in anodic alumina," *Applied Physics Letters*, vol. 71, no. 19, pp. 2770–2772, 1997. doi:10.1063/1.120128
- [27] A Santos, L Vojkuvka, M Alba, VS Balderrama, et al. " Understanding and morphology control of pore modulations in nanoporous anodic alumina by discontinuous anodization", *Physica Status Solidi (a)* vol. 209, no. 10, pp. 2045-2048, 2012. DOI: 10.1002/pssa.201228150
- [28] A Santos, J Ferré-Borrull, J Pallarès, LF Marsal, "Hierarchical nanoporous anodic alumina templates by asymmetric two-step anodization", *Physica Status Solidi (a)* vol. 208, no. 3, pp. 668-674, 2011. DOI: 10.1002/pssa.201026435
- [29] O. Jessensky, F. Müller, and U. Gösele, "Self-organized formation of hexagonal pore structures in anodic alumina," *Journal of The Electrochemical Society*, vol. 145, no. 11, pp. 3735–3740, 1998. doi:10.1149/1.1838867
- [30] H. Takahashi and M. Nagayama, "The determination of the porosity of anodic oxide films on aluminium by the pore-filling method," *Corrosion Science*, vol. 18, no. 10, pp. 911–925, 1978. doi:10.1016/0010-938x(78)90012-4
- [31] M. Porta-i-Batalla, E. Xifré-Pérez, and C. Eckstein, "3D nanoporous anodic alumina structures for sustained drug release," *Nanomaterials*, vol. 7, no. 8, p. 227, 2017. doi:10.3390/nano7080227
- [32] B. Zhou and W. F. Ramirez, "Kinetics and modeling of wet etching of aluminum oxide by warm phosphoric acid," *Journal of The Electrochemical Society*, vol. 143, no. 2, pp. 619–623, 1996. doi:10.1149/1.1836489
- [33] K. Ersching, E. Dorico, and R. C. da Silva, et al., "Surface and interface characterization of nanoporous alumina templates produced in oxalic acid and submitted to etching procedures," *Materials Chemistry and Physics*, vol. 137, no. 1, pp. 140–146, 2012. doi:10.1016/j.matchemphys.2012.08.058
- [34] S. Lamouri, M. Hamidouche, and N. Bouaouadja, "Control of the γ -alumina to α -alumina phase transformation for an optimized alumina densification," *Boletín de la Sociedad Española de Cerámica y Vidrio*, vol. 56, no. 2, pp. 47–54, 2017. doi:10.1016/j.bsecv.2016.10.001
- [35] M. Porta-i-Batalla, E. Xifré-Pérez, and C. Eckstein, "3D nanoporous anodic alumina structures for sustained drug release," *Nanomaterials*, vol. 7, no. 8, p. 227, 2017. doi:10.3390/nano7080227